EUROPEAN ORGANIZATION FOR NUCLEAR RESEARCH

EN/MME/Metallurgy

UNIVERSIDAD CARLOS III DE MADRID

Materials Science and Engineering Department

PROYECTO FIN DE CARRERA

Characterization of materials and welded interfaces for the SPL Project

Author: Ignacio Aviles Santillana

Director: Elisa Maria Ruiz Navas

Supervisor CERN: Gonzalo Arnau Izquierdo

Madrid - December 1, 2011

Preface

First of all, I would like to apologize if this preface is too long. I have always thought that it is the most important part of a work like this which closes an important part of your life.

I would like to thank Dr Elisa Ruiz for the time she dedicated to me and for supporting me in this little adventure.

My thanks go also to Dr. Stefano Sgobba and Mr. Gonzalo Arnau Izquierdo for giving me the opportunity of conducting such an interesting study in a cutting - edge research center as CERN is. I would also like to thank all the members of the SPL project for their patience and continuous support. Special mention to Dr. Ofelia Capatina, Mr. Said Atieh, Mr. Gonzalo Arnau Izquierdo and Mrs. Nuria Valverde Alonso.

To the materials section here at CERN I only have words of gratitude. It is amazing how such a recognized experts in their fields can be so attentive, patient and understanding with a student. To Gonzalo Arnau Izquierdo and Stefano Sgobba, all your advises were an inspiration to me. To Philippe Deweulf for all the good times together. To Jean Michel Dalin, always willing to help me and to share a laugh. To Anite Perez, for her perpetual good mood. Aline Piguiet and Maud Scheubel, not only colleagues but friends. To Miguel Gil for sharing with me this adventure from the very beginning. To Dawid Marcinek, president of the PhD students of the University of Krakow, husband, father... and friend. To Alexandre Gerardin: if I was French, I would like to be like you. And at last, but not least, to Dr. Markus Aicheler, my German bro' for whom I don't have enough words of gratitude.

Thanks to all my family that made me the way I am. My parents, my three elder sisters (and brothers in law), my younger one, and my aunt. You have always been a model to me. I owe you everything.

To my friends of school. There is no single day that you don't appear in my conversations. I am so proud of all of you and of being your friend.

To my friends of university, for millions of good moments, exams, coffees, afternoons in Leganes... Special mention has to be done to Joaquin Garcia (and family). I am sure that without you, all of this would have been a lot different. You really made the difference. In the end 'acabo bien'.

And at last, but not least, to the most outstanding person I have ever met: Alejandra. You simply make me a better person.

Contents

Nomenclature

Acronyms

ASM	American Society for Metals
CERN	European Organization for Nuclear Research
DESY	Deutsches Elektronen - Synchrotron
DPI	Dye Penetrant Inspection
EB	Electron Beam
EBW	Electron Beam Welding
EDM	Electrical Discharge Machining
EDS	Energy - Dispersive X - Ray Spectrometry
EP	Electropolishing
fcc	face centered cubic
FE	Field Emission
HAZ	Heat Affected Zone
HOM	High Order Modes
HPWR	High Pressure Water Rinsing
HT	Heat Treatment
HV	Vickers Hardness
LHC	Large Hadron Collider

Linac	Linear Accelerator
NDT	Nondestructive Testing
OFE	Oxygen Free Electronic
RIB	Radioactive Ion Beam
RRR	Residual Resistivity Ratio
SC	Superconductive
SCRF	Superconducting Radio Frequency
SEM	Scanning Electron Microscope
SPL	Superconductive Proton Linac
SS	Stainless Steel
TESLA	Tera-electronvolt Energy Superconducting Linear Accelerator
UT	Ultrasonic testing
UTS	Ultimate Tensile Strength

Greek Symbols

Δl	Variation of length	mm
ϵ	Strain	%
λ	Wavelength	m
μ	Linear absorption coefficient	mm^{-}1
σ	Stress	MPa

Latin Symbols

a	Lattice parameter	Å
A_o	Initial section	mm^2

d	mean of the two diagonals of the Vickers indentation	mm
F	Force	N
I	Intensity	mA
I_o	Incident intensity	mA
l_i	Final Length	mm
l_o	Initial Length	mm
E	Young Modulus	GPa

1. Introduction

1.1. CERN

CERN, the European Organization for Nuclear Research, is one of the worlds largest and most respected centers for scientific research. Its business is fundamental physics, finding out what the Universe is made of and how it works. At CERN, the worlds largest and most complex scientific instruments are used to study the basic constituents of matter: the fundamental particles. By studying what happens when these particles collide, physicists learn about the laws of Nature [1]

The instruments used at CERN are particle accelerators and detectors. Accelerators boost beams of particles to high energies before they are made to collide with each other or with stationary targets. Detectors observe and record the results of these collisions. An schematic representation of the CERN accelerator complex can be seen inf Figure 1.1.

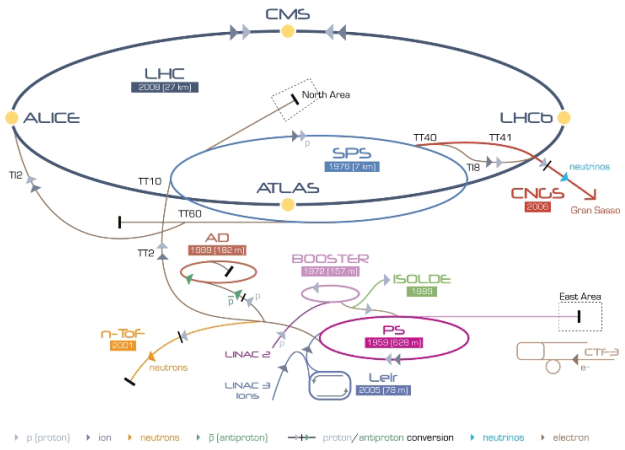

Figure 1.1.: The CERN accelerator complex [1]

1.2. SPL project

The existing complex of accelerators at CERN is capable to provide the Large Hadron Collider (LHC) with the beam required to reach its nominal characteristics. Higher performance injectors will however be necessary to exceed this limit and maximize the physics reach of the LHC [2]. A first proposal for building a Superconductive Proton Linac (SPL) at CERN to replace some of the existing accelerators was reported 14 years ago [3] with the potential for evolving towards very high beam power which would support new physics facilities for neutrinos and/or Radioactive Ion Beams (RIB) [2]. Later, the design of the SPL evolved towards a low-power 4 GeV version (LP-SPL), with potential use as a new injector chain for the LHC, with the Linac4, presently under construction, as a low energy front-end linac, and having the potential to be up-graded to a multi-MW proton injector [2].

Following recent changes in the mid-term plan strategy at CERN, the construction of the LP-SPL has been stopped, but the continuation of the R&D effort towards a high-power version of the SPL has been endorsed [4]. The SPL project, coordinated by CERN in partnership with other international laboratories aims at developing key technologies for the construction of a multi-megawatt proton linac (Figure 1.2) which would serve as a driver for new physics facilities such as neutrinos and RIB.

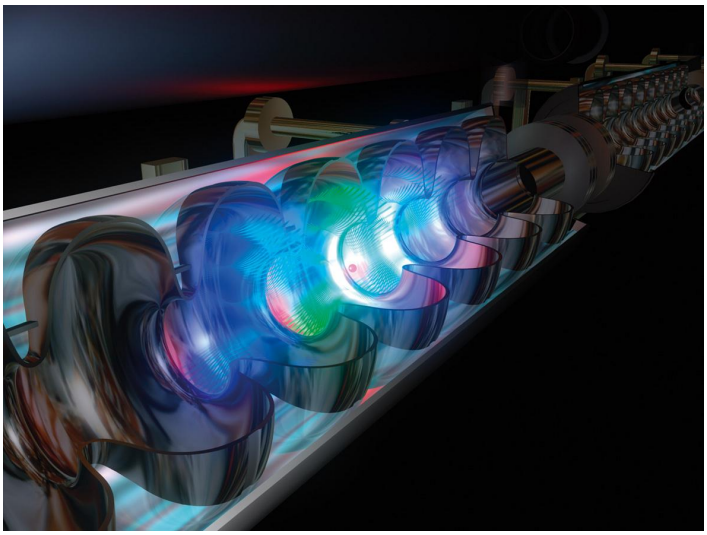

Figure 1.2.: Recreation of a particle being accelerated by a linac [5].

2. State of the Art

This chapter introduces the present knowledge on which this study is based on. In a first part, it presents a short introduction to the present status of the SPL project. Then, some facts about niobium are found to end with a description of the current way to join niobium to titanium.

2.1. A brief description of the SPL Project

As one of the priorities of the high power version of the SPL program, 704 MHz bulk niobium β=0.65 and β=1 elliptical cavities are to be developed and tested at IPN Orsay, CEA Saclay and CERN. High purity niobium with a value of the Residual Resistivity Ratio (RRR) greater than 300 will be used in order to achieve the desired accelerating gradients [6]. In an initial phase, at CERN, four β=1 cavities will be supplied, and will need to be tested together as they would operate in a cryo-module. Figure 2.1 presents the cavity together with its helium tank, the main coupler, the High Order Modes (HOM) coupler, the tuner and the cold magnetic shielding, in the configuration that will be tested at CERN in the cryo-module. The main properties of the β=1 cavities are summarized in Table 2.1, for a 50 Hz pulsed operation, 20 mA current and 0.8 ms beam pulse length.

2.1.1. Cavity Geometry

A multicell resonator is advantageous for maximizing the active acceleration length in a linac of a given size. With the increasing number of cells per cavity, however, difficulties arise from trapped modes, uneven field distribution in the cells, and too high power requirements on the input coupler, so a 5 cell structure was decided by CEA Saclay [7].

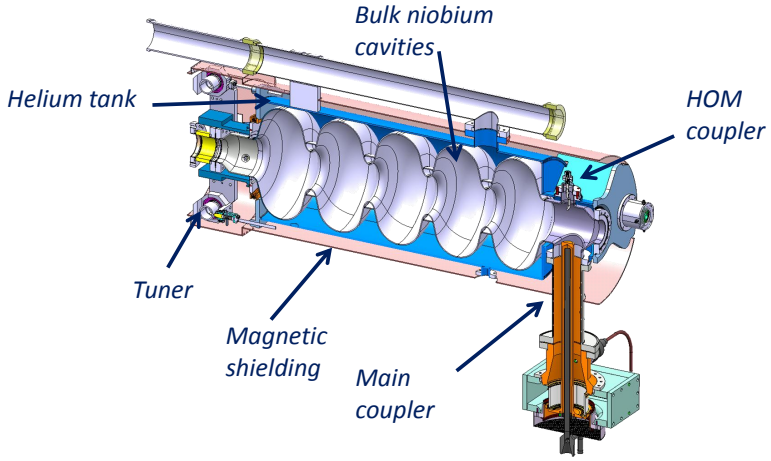

Figure 2.1.: Schematic sectional view of the five-cell cavity inside its hellium tank with the power coupler and HOM coupler (right) and pick up probe port, transition bellows and tuner (left) [4]

Property	Value
Cavity material	bulk niobium
Gradient/(MV/m)	25
Quality factor Q_o	$10{\cdot}10^9$
R/Q /(Ω)	570
Operating Temp./ (K)	2

Table 2.1.: β=1 cavity, main properties and operation [4]

The design of the cell shape was guided by the minimization of electric and magnetic fields at the cavity walls to reduce the danger of field emission and thermal breakdown and also by the need of a spherical contour near the equator with low sensitivity for multipacting [8].

The resonator is operated in the π mode so the longitudinal dimensions are determined by the condition that the electric field has to be inverted in the time a relativistic particle takes to travel from one cell to the next. The separation between two irises is therefore $c/(2f)$.

The cavity is asymmetrical as it can be seen in Figure 2.2. The drift tube at the right of the figure has a diameter of 140 mm, necessary to receive the

fundamental power coupler which has a 100 mm diameter. The second drift tube will host the tuning system and 130 mm diameter is enough. The diameter is reduced at both sides to 80 mm for the connection between two adjacent cavities, provided by flanges [4].

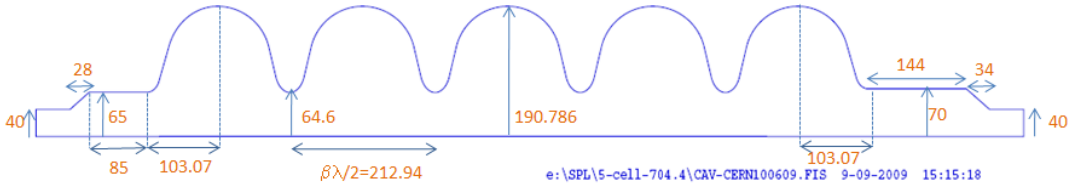

Figure 2.2.: Geometrical parameters of the β=1 cavity [4]

2.1.2. Mechanical design

The mechanical design of the cavities ensures their safe use under maximum loading condition during its entire lifecycle. Since these cavities are aimed to work in the pulsed mode, the sensitivity to the Lorenz force is also especially critical. The effects of the detuning due to those forces were limited by adding stiffening rings in-between the inner cavity half-cells. Figure 2.3 present a qualitative comparison between the mechanical deformation of the cavity with and without stiffening rings, under the effect of the Lorentz forces induced by the electromagnetic field. The absolute value of its scales is the same in both cases.

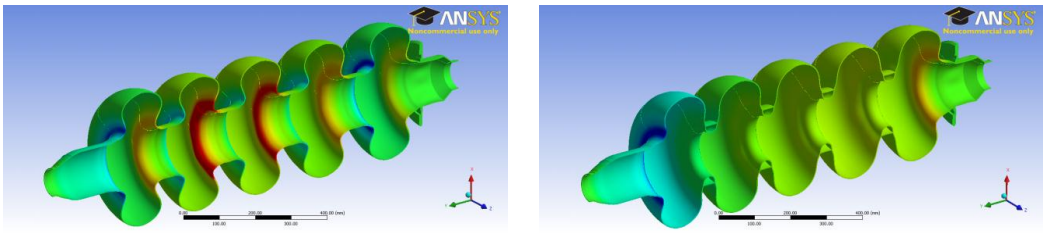

Figure 2.3.: Figure 2.3a shows the cavity without stiffening rings deformed due to Lorentz forces. Figure 2.3b shows the cavity with the stiffening rings deformed due to Lorentz forces [4].

A final thickness of 3 mm was calculated to be acceptable in order to cope

with all the mechanical constraints as well as minimizing the costs of the cavity production.

2.2. High Purity Niobium for SC cavities

The name niobium comes from Niobe, daughter of Tantalus in the Greek mythology, as niobium is often associated with tantalum [9]. Formerly known as Columbium, from Columbia, America, the original source of niobium ore. Many metallurgists, metal societies, and commercial producers still use the name Columbium.

Platinum-white with a bright metallic luster, it takes on a bluish cast when exposed to air at room temperatures for a long time. Niobium is ductile, malleable, and highly resistant to corrosion. It is mostly used for superconductive (SC) cavities because:

- its high transition temperature (9.2 K, the highest of elemental superconductors)
- its high critical magnetic field (240 mT)
- possibility to machine it and spin it or deep drawn it
- availability as bulk and sheet material in any size

In addition, it is one of three elemental superconductors that are type II.

But it was not until the purification techniques of niobium were improved that it started to be used as bulk material for SC cavities, because in order to achieve the highest accelerating gradients, very high purity niobium is needed. Electron Beam (EB) purification together with the most careful surface preparation and cleaning by means of Electropolishing (EP) and High Pressure Water Rinsing (HPWR) respectively have made niobium becomes the workhorse in the production of SC cavities.

2.3. Titanium for the helium tank

The search for suitable materials for cryogenic service is the search for materials which, under service conditions (in this particular case temperatures of about

2 K), have adequate strength, ductility and fracture toughness [10]. The advantages of titanium alloys are high strength, high specific strength, and low thermal conductivity as it can be seen in Table 2.2 for pure titanium and a common titanium alloy. On the other hand they have the disadvantage of a lower fracture toughness than other fcc metal under the same conditions [10].

Property	Titanium	Ti6Al4V
UTS / (MPa)	345 – 490	862 – 1200
Specific UTS / ($MPa \cdot m^3 \cdot Kg^{-1}$)	0.076 – 0.108	0.195 – 0.272
Thermal conductivity / ($W \cdot m^{-1} \cdot {}^{\circ}C^{-1}$)	16.3 – 18	7.1 – 7.3

Table 2.2.: Properties of titanium and a common titanium alloy [11]

Eventhough it is not the easiest nor the cheapest solution, helium tank in titanium was chosen because of its similar coefficient of thermal contraction as niobium, international proven technology and because the tuner designed by CEA is thought for this material [12].

An alloyed version of titanium was preferred to pure titanium, even if the pure one is more 'classically' used in other Institutes as material of helium tanks hosting RF cavities. Grade 5 titanium (Ti6Al4V) is significantly stronger than the commercially pure titanium, while having the same stiffness and thermal properties. This grade is heat treatable, already used in many cryogenic applications and is an excellent combination of strength, corrosion resistance and weldability [10]. Its mechanical properties allow also its use for the manufacturing of ConFlat flanges, cheaper than the NbTi flanges usually utilized when titanium helium tanks are chosen [4].

2.4. Niobium - Titanium Electron Beam Welding with Intermetallic Transition

One of the driving elements for the mechanical design of the equipped cavity were the transitions from the helium tank to all the adjacent components. Figure 2.4 shows the interfaces that need to be defined.

Between all these transitions, some of them are between Stainless Steel (SS)

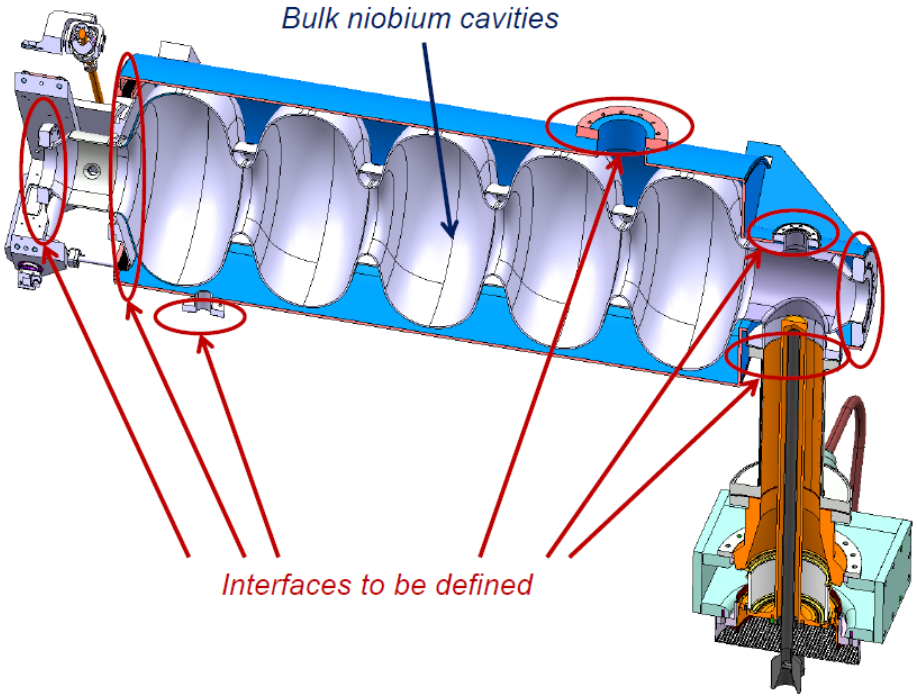

Figure 2.4.: SPL β=1 equipped cavity with the interfaces to be defined.

and titanium, and the best solution for them is found to be through flanges and helicoflex sealing [12].

For the joint between the helium tank and the cavity, a transition between titanium and niobium needs to be defined. The Tera-electronvolt Energy Superconducting Linear Accelerator(TESLA) cavities currently under development at the Deutsches Elektron-Synchrotron (DESY) chose a solution which consists in a conical disc of a Nb - Ti alloy (more preciselly Nb55Ti) between the titanium transition ring and the niobium connecting flange (Figure 2.5). Both extremities of the conical disc would be EB welded. With this configuration, the EB welding process will be first between niobium and NbTi and second between titanium and NbTi, and never between niobium and titanium directly. The material of the flanges would be also manufactured with the same niobium - titanium alloy as explained in [13].

This particular choice was motivated by the stability of the mechanical properties after a 1400°C heat treatment carried out to increase the RRR values and

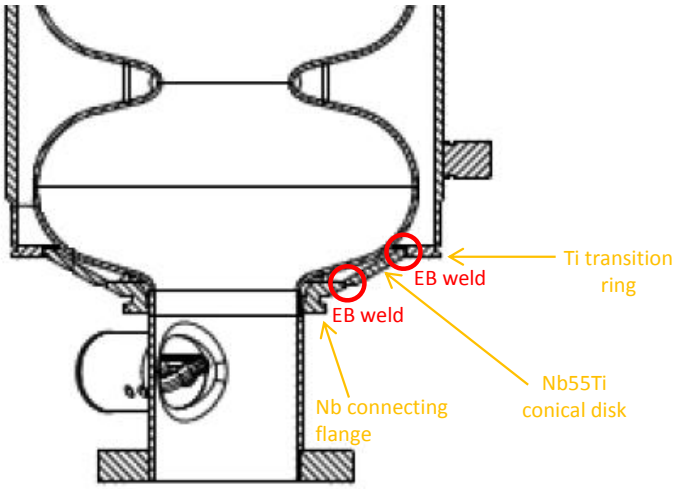

Figure 2.5.: Extremity of a dressed TESLA cavity showing the weld joint geometry [14].

to homogenize the material [13]. But recent investigations show that a 1400°C heat treatment is no longer needed and a 2h 800°C degassing is proven to be enough in order to achieve the desired properties [15].

3. Motivation and Objectives

The SPL project is an R&D effort coordinated by CERN in partnership with other international laboratories, aimed at developing key technologies for the construction of a multi-megawatt proton linac based on state-of-the-art RF superconducting technology, which would serve as a driver for new physics facilities such as neutrinos and RIB. The Materials and Mechanical Engineering group of CERN aims for 2013 the construction of a string of 4 bulk niobium β=1 elliptical cavities, operating at 2 K with a very ambitious accelerating gradient of 25 MV/m.

In order to achieve such a high gradient, bulk high purity niobium is required because of its unique properties in terms of critical superconductive temperature, critical magnetic field and formability. The highly restrictive technical specifications proposed by CERN can not be fulfilled by much companies, so a full material characterization needs to be done with advanced techniques such as RRR measurements and more conventional ones like tensile testing for the determination of the mechanical properties.

Therefore, in this work, a full qualification of a prototype piece from the firm PLANSEE was done to determine if the values satisfied the requirements for the manufacturing and operation of a SCRF cavity with the proposed parameters. It will be also studied the degradation of purity of niobium as a consequence of the electron beam welding processes that the cavity will undergo during its manufacturing and assembly.

Additionally, the R&D program conducted by a team of CERN specialists explores new mechanical design and new fabrication methods for the elliptical β=1 cavities fabricated from niobium sheets . One of the main points of this program is the definition of the interfaces of the cavity and the helium tank, and therefore require careful studies and qualification of applicable joining techniques.

Hence, in this work the feasability of an electron beam butt weld of high purity niobium and Ti6Al4V alloy was studied. The main objective was to determine if the joint fulfilled the requirements for the designed interfaces, what was done via non-destructive and mechanical testing. In parallel, more tests were carried out to study the aspect of the weld, its microstructure and its composition, what is of great interest from a point of view of understanding the behavior of the joint during the welding process.

4. Material Characterization Techniques

This chapter describes the non–destructive characterization methods used, followed by an explanation of the destructive ones in the form of descriptions, figures and equations. The chapter closes with a brief description of the EBW technique.

4.1. Non-Destructive

The American Society for Metals (ASM) defines Non-destructive testing as follows[16]: "Nondestructive testing or Non-destructive testing (NDT) is a wide group of analysis techniques carried out in a material which do not change in a permanent way its physical, chemical, mechanical or dimensional properties". NDT involves negligible or no damage.

In the following, there will be explained the NDT techniques used in this work, sometimes because it was stated like this in the standards and sometimes because it was considered the most suitable technique to characterize certain property of the material.

4.1.1. Radiographic inspection

Radiology is the general term given to material inspection methods that are based on the differential absorption of penetrating radiation by the testpiece being inspected [17]. Because of differences in density, variations in thickness and differences in absorption characteristics caused by variations in composition, different parts of a testpiece absorb different amounts of penetrating radiation according to

$$I = I_o exp(-\mu t) \tag{4.1}$$

where I is the intensity of the emergent radiation, I_o is the incident intensity, t is the thickness of the homogeneous material, and μ is a characteristic of the material known as linear absorption coefficient.

Principles of Radiography

There are three basic elements in a radiographic analysis: radiation source, testpiece (which we will suppose it has a flaw) and sensing material. In order to obtain an interpretable image, radiation from the source is absorbed by the testpiece as the radiation passes through it. The flaw and the surrounding material absorb different amounts of radiation and thus, the intensity of the radiation that impinges on the sensing material in this area is different from the adjacent areas. This produces a contrast image as seen schematically in Figure 4.1.

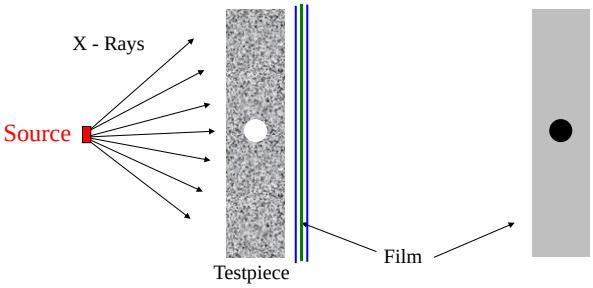

Figure 4.1.: Schematic of the basic elements of a radiographic system showing the method of sensing the image of an internal flaw in a plate of uniform thickness

These variations can be monitored by detecting the unabsorbed radiation that passes through the testpiece. Because of that it can be said that radiography is used to detect the features of a component or assembly that exhibit a difference in thickness or density compared to surrounding material [17].

4.1.2. Dye Penetrant Testing

Dye penetrant inspection (DPI) is a widely used method for the detection of surface discontinuities of any kind of non porous material. It is non destructive test based on the capillarity of fluids, so it is limited to the detection of surface discontinuities or subsurface defects with surface openings [18]

Penetrant inspection depends on the ability of the liquid to wet the surface of the material and to introduce itself inside the cavities opened to the surface in a reasonable amount of time. Thus, the desirable characteristics that a liquid penetrant should have are: high capillarity, so that the liquid depresses or rises from the narrow surface cavities; low surface tension, so that the liquid wets the surface of the material; and low viscosity, so that the liquid flows quickly enough over the surface and inside the cracks [19].

The first indispensable condition is a clean and dry surface, as any contamination may hamper the wetting of the surface cracks. After this, the liquid penetrant is applied to the whole surface so that a homogeneous coating all over the test surface is achieved. The liquid needs to stand for a short period of time (known as dwell time) over the surface so that it is absorbed by the surface discontinuities by capillarity action. After the dwell time has elapsed, excess penetrant is removed, leaving some trapped penetrant inside the surface cracks. Finally, a developer is applied to the surface that extracts the penetrant from the surface defects. As the crack forms a volume in depth filled with the penetrant liquid, the developer absorbs all the liquid contained inside it. Thus, the indication of the existence of a defect is much wider than the actual surface discontinuity, making it this way much easier to detect [18].

4.1.3. Ultrasonic Inspection

Sound is a pressure wave traveling with a velocity depending on the mechanical properties of the medium. Imperfections and inclusions cause sound waves to be scattered, resulting in echoes, reverberations and general dampening of the sound wave. The detection of the reflected or transmitted waves permits defects to be located [16].

In ultrasonic testing (UT), very short ultrasonic pulse-waves are launched into materials to detect internal flaws or to characterize materials' homogeneity. In

UT, an ultrasound transducer connected to an oscilloscope is passed over the object to be inspected. There must not be discontinuities between the transducer and the specimen's surface, so a coupling agent is normally used between them to reduce the losses in the ultrasonic wave energy due to separation between the surfaces.

According to the way of receiving the ultrasonic wave there can be found two different methods: reflection and attenuation. In reflection (or pulse-echo) mode (Figure 4.2), the transducer performs both the sending and the receiving of the pulsed waves. Reflected ultrasonic waves arise from an interface, such as the back wall of the object or from an imperfection within the object. The oscilloscope displays these results in the form of a signal: its amplitude represents the intensity of the reflection and its distance represents the arrival time of the reflection.

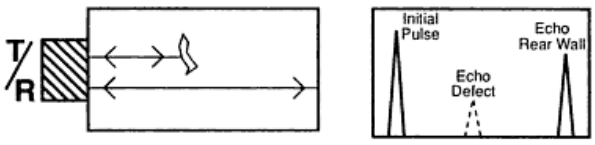

Figure 4.2.: Pulse - eco mode in UT [20].

In attenuation (or through-transmission) mode (Figure 4.3), a transmitter sends ultrasounds through one surface, and a separate receiver detects the amount that has reached it on another surface after traveling through the medium. Imperfections or other conditions in the space between the transmitter and receiver reduce the amount of sound transmitted, thus revealing their presence [20].

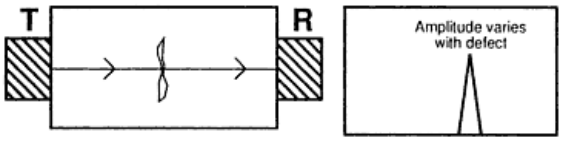

Figure 4.3.: Attenuation mode in UT [20].

4.1.4. Roughness

The state of the surface of a material is of paramount importance for some applications as it plays an important role in determining how a real object will interact with its environment. Historically, the roughness profile and its parameters have been the only parts of surface texture characterization that have been well defined.

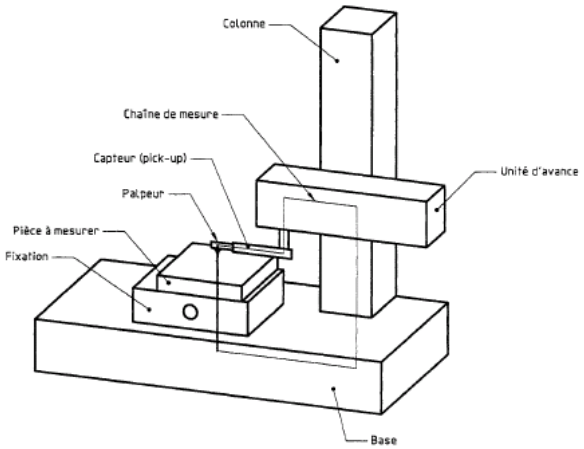

Figure 4.4.: Representation of a contact roughness tester

The measuring principle is as follows (see Figure 4.4): A stylus-type 'shoe sensor' comes in contact with the workpiece and moves along a straight profile. This probe, via an inductive sensor transforms the mechanical probing (variation of height) into an electrical signal which is then sent to a computer to show the measured profile. From this profile, signal processing is performed using bandpass filters.

4.2. Destructive

In destructive testing, the objective is to understand and observe a specimen's structural performance or its behavior under different stress factors to the point it fails. They are normally easier and yield more information than NDT, but they require the sacrifice of one or more samples.

4.2.1. Optical microscopy

With optical microscopy, the light microscope is used to study the microstructure; optical illumination systems are its basic elements and therefore, its resolution power (ability to distinguish between to adjacent points) is limited by the visible light's wavelength. Contrasts in the image produced result from differences in reflectivity of the various regions of the microstructure. Careful and meticulous surface preparations are necessary to reveal the important details of the microstructure. The specimen surface must first be ground and polished to a smooth and mirror like finish. The microstructure is revealed by a surface treatment using an appropriate chemical reagent (etching). The atoms at the grain boundaries are chemically more active, and consequently dissolve more readily than those within the grains forming small grooves. These grooves become discernible when viewed under a microscope because they reflect light at an angle different from that of the grains themselves.

4.2.2. SEM

A scanning electron microscope (SEM) is a type of electron microscope that images a sample by scanning it with a high-energy beam of electrons in a raster scan pattern. It uses a beam of electrons to obtain information of the surface of a sample so while the resolution of an optical microscope is limited by the wavelength of visible light, the electron microscope's resolution is limited by both the wavelength of the electrons and the volume of the material being excited by the beam (the interaction volume). The more volume is excited, the worse resolution can be obtained, so a compromise solution should be found between a lower wavelength obtained with higher accelerating fields and lower interaction volumes obtained with lower accelerating fields. According to [21], the critical term for resolution is the excited volume so in order to have a better resolution, the lowest accelerating voltages should be used.

How SEM works

Figure 4.5 show a scheme of how a SEM works. Free electrons are formed in the electron gun and accelerated through a potential field that can vary from

0.1 - 30 kV. After that, the beam goes through different sets of magnetic lenses in order to focus it on the sample's surface and is then deflected by means of the scan coils, which deflect the beam in the x and y axes so that it scans in a raster fashion over a rectangular area of the sample surface.

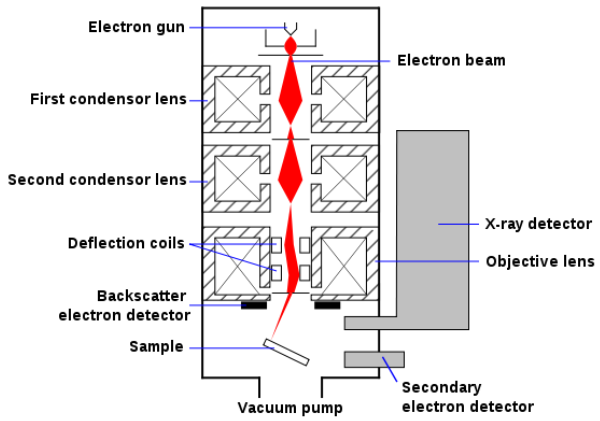

Figure 4.5.: Schematic diagram of an SEM [22].

When the electron beam interacts with the sample, the electrons lose energy by repeated random scattering and absorption with the interaction volume. The energy exchange between the electron beam and the sample results in the reflection of high-energy electrons by elastic scattering (Backscattered electrons), emission of secondary electrons by inelastic scattering and the emission of electromagnetic radiation. Each of this signals can be detected by specialized detectors.

4.2.3. Energy - Dispersive X - Ray Spectrometry

Energy-Dispersive X-ray Spectrometry (EDS) detects the photons that come out of the sample when hit by the electron beam of the SEM to determine the composition of the specimen in both qualitative and quantitative way. Two different kinds of photons are emitted: The characteristic X-rays, which are the ones used to identify the composition of the sample because of its unique relation with the atomic structure of the elements; and the continuum X-rays, which appear because of the decelerating process experienced by the electron beam constituting a background in the spectra.

Characteristic X - Ray production

When the electron beam strikes the sample specimen, it can extract an electron from an inner shell, leaving the atom in an excited energetic state with a missing inner shell electron. Since the excited atomic shell aims at the equilibrium, the atom relaxes to the smallest internal energy (the ground state), filling the inner shell vacancy through a transition of an outer shell electron. As the electron in the higher level is more energetic, the excess of energy can be released from the atom in two different ways: the Auger process, in which the difference in energy is transmitted to another outer shell electron ejecting it from the atom; and the characteristic x-ray process, in which the difference in energy results in the emission of a photon of electromagnetic radiation whit a defined energy. The energy difference between electron shells is a characteristic value of each element [23].

Continuum X - Ray production

Every time charged particles are accelerated or braked, they produce electromagnetic radiation. The Coulombic field of the specimen atoms (which is the positive field of the nucleus and the negative field of the bound electrons) can make the electron beam undergo a deceleration process, in which the energy loss in the electron is traduced in a photon emission. The energy of this photon is $\Delta E = h\nu$, where h is Planck's constant and ν is the frequency of the electromagnetic radiation. This radiation is best known as bremsstrahlung [23]. As the interactions between the specimen and the electron beam are random, the electron can lose any amount of energy in each deceleration event. Thus, the energy of the bremsstrahlung (Figure 4.6) can take any value from zero to the original incident energy, forming a continuous electromagnetic spectrum [23].

The intensity of this spectrum is important in analytical x-ray spectrometry because it forms a background under the characteristic peaks. Once a photon is created, it is impossible to determine whether it is a continuum or a characteristic x-ray. Thus, the background intensity occurring at the same energy as a characteristic x-ray sets a limit to the minimum amount of an element that can be detected [23].

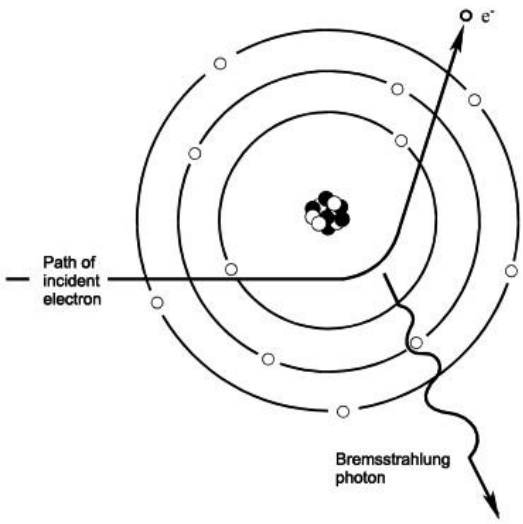

Figure 4.6.: Schematic representation of the origin of the Bremsstrahlung[23]

Quantitative analysis (ZAF)

The principle in which this analysis underlies is the comparison between the characteristic x-ray intensity for a given element and that measured from a known standard. The ratio between the two should be equal to the ratio of concentrations for a given element between the specimen and the standard, what can be expressed as the following equation:

$$\frac{C_i}{C_(i)} = \frac{I_i}{I_(i)} = k_i \tag{4.2}$$

The terms C_i and $C_(i)$ are the composition in weight concentration of element i in the sample and in the standard respectively. The ratio $I_i/I_(i)$ is the basic experimental measure which lies beneath every quantitative x-ray microanalysis, and has the special designation of k ratio [23]. It represents the ratio between the intensity of the sample and the one for the standard after the continuum background is subtracted.

But equation 4.2 is an idealization for a sample with no other interaction than the electron beam. In quantitative analysis of actual samples we have to consider that the generation of a photon of an element affects its surroundings.

These alterations are known as matrix effects, and their physical origin is well understood [24]. It is convenient to divide them into atomic number (Z_i), x-ray absorption (A_i) and x-ray fluorescence (F_i), the so know ZAF factors. In this sense, the above mentioned k ratio needs to be corrected using the ZAF factors, hence leaving equation 4.2 as:

$$\frac{C_i}{C_(i)} = [ZAF]_i \cdot \frac{I_i}{I_(i)} = [ZAF]_i \cdot k_i \tag{4.3}$$

4.2.4. Tensile Test

Tensile test is probably the most fundamental type of mechanical test that can be performed on a material. Important design properties of materials can be determined by this test, such as ultimate tensile strength (UTS), elastic limit or Young's modulus. The procedure is simple: the sample is clamped from its extremities to the tensile tester and an increasing traction load is applied uniaxially along its axis. Instant load and elongation are measured simultaneously with a load cell and an extensometer respectively. The test ends when the sample is unable to withstand the applied load and consequently fractures.

The instant load and the elongation data gathered is normalized so that it is not specific to the geometry of the test sample. Operating this way, two new parameters are defined: nominal stress and nominal deformation. Nominal stress is defined by the relation

$$\sigma = \frac{F}{A_o} \tag{4.4}$$

Where σ is the nominal stress in megapascals (1MPa = 10^6 N/m^2), F is the instant force applied perpendicularly to the section of the sample in Newton (N), and A_o is the area of the original section before applying the load in square millimeters (mm^2).

Nominal deformation is defined as

$$\epsilon = \frac{l_i - l_o}{l_o} = \frac{\Delta l}{l_o} \tag{4.5}$$

where l_o is the original length before applying the load, and l_i is the instant longitude, so that Δl represents the change in longitude in a determined instant with respect to the initial longitude. Nominal deformation has no units, but it is commonly expressed in percentage.

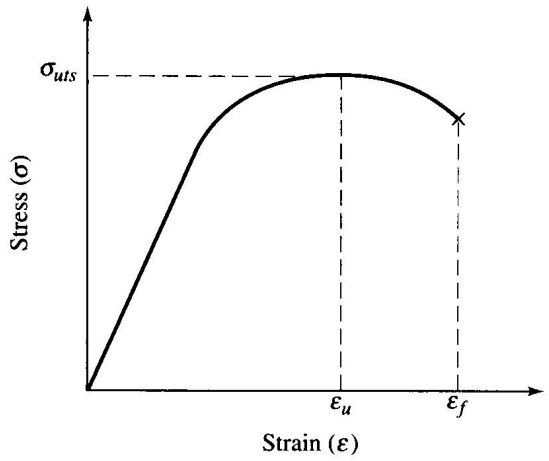

Figure 4.7.: Stress - Strain curve

From this curve (Figure 4.7), the parameters UTS, maximum elongation and reduction in area can be directly observed. Other important properties can be calculated using of the curve, such as Young's Modulus (E), elastic limit, ductility or toughness [25].

4.2.5. Hardness Test

'Hardness is a measure of the resistance of a material to localized plastic deformation when it is subject to a force' [25]. The behavior of solid materials under force is complex; hence there are different measurements of hardness. The most usual type of hardness in metallurgy is the indentation hardness, which measures the resistance of a sample to permanent plastic deformation or plastic flow of the material due to a constant compression load for a definite period of time. The size or the depth of the indentation is measured, what it is afterwards related with a hardness number [26]. The most frequent hardness tests are Brinell, Vickers and Rockwell. In this work, Vickers hardness was measured with the help of a Wolpert 2RC device. For further information about the other two techniques go to [26].

Vickers Hardness

Vickers hardness (HV) is a measure of the hardness of a material calculated from the size of the impression produced under load of a diamond indenter. Its geometry is the one of a square - based pyramid with an angle in the apex of 136° [27]. The indenter is pressed into the surface for a determined period of time, and, when removed, the length of the diagonals of the impression is measured with the assistance of a calibrated microscope. HV is then calculated by means of the following formula:

$$HV_x = \frac{0.189F}{d^2} \tag{4.6}$$

where HV is the value of the Vickers Hardness, x represents the load used during the test in kilograms, F is the load used during the test in Newton and d is the mean of the two diagonals of the indentation.

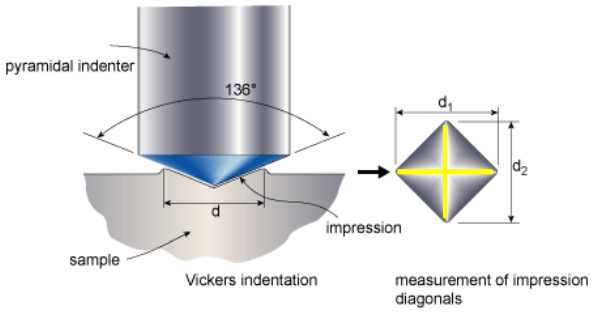

Figure 4.8.: Schematic of a Vickers indentation and its measurement

4.2.6. X-Ray Diffraction

X-rays are electromagnetic radiation with typical photon energies in the range of 100 eV - 100 keV. For diffraction applications, only short wavelength x-rays in the range of 1 keV - 120 keV are used. Because the wavelength of x-rays is comparable to the size of atoms, they are ideally suited for probing the structural arrangement of atoms and molecules in a wide range of materials. The energetic

x-rays can penetrate deep into the materials and provide information about the bulk structure.

X-rays primarily interact with electrons in atoms. When x-ray photons collide with electrons, some photons from the incident beam will be deflected away from the direction where they originally travel. If the wavelength of these scattered x-rays did not change (meaning that x-ray photons did not lose any energy), the process is called elastic scattering (Thompson Scattering) in that only momentum has been transferred in the scattering process [28]. These are the x-rays that are measured in diffraction experiments, as the scattered x-rays carry information about the electron distribution in materials. On the other hand, in the inelastic scattering process (Compton Scattering), x-rays transfer some of their energy to the electrons and the scattered x-rays will have different wavelength than the incident x-rays.

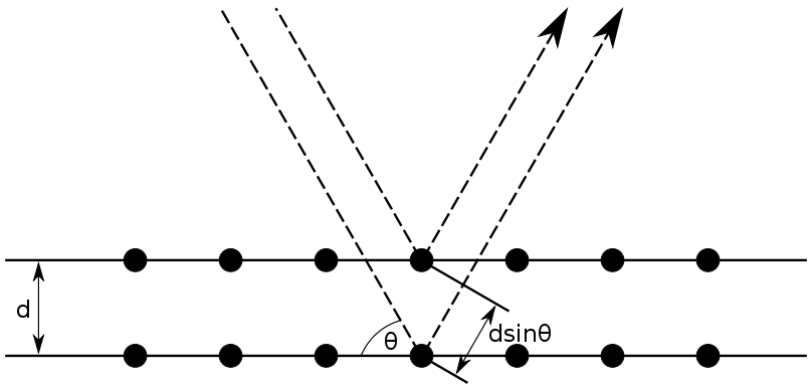

Figure 4.9.: Bragg diffraction. Two beams with identical wavelength and phase approach a crystalline solid and are scattered off two different atoms within it

Diffracted waves from different atoms can interfere with each other and the resultant intensity distribution is strongly modulated by this interaction. If the atoms are arranged in a periodic fashion, as in crystals, the diffracted waves will consist of sharp interference maxima (peaks) with the same symmetry as in the distribution of atoms [28]. The maximum intensity at the so called 'Bragg angles' indicate that Bragg's conditions are met. According to Bragg's law

$$n\lambda = 2a \sin\theta \tag{4.7}$$

each *Bragg angle* θ corresponds to a certain distance between the lattice planes (*lattice parameter a*) linked through the *wavelength* λ of the X-Rays. When Bragg conditions are met, constructive interference occurs and a strong signal is diffracted (Figure 4.9). Through the measurement of the *lattice parameter a* and a database with diffraction patterns, it is possible to identify different chemical and crystallographical phases.

4.2.7. Residual Resistivity Ratio (RRR)

Residual Resistivity Ratio (RRR) is defined as the ratio between the resistance of a sample at room temperature (298 K) and the resistance of the sample just above its transition temperature ($\tilde{9}$.5K) [29] or at 4.5 K in normal conducting state by applying an external magnetic field. Another possibility is measuring the RRR at several different temperatures above its transition temperature and then extrapolate the values to 4.5 K The opposition to the flow of electrons across a high-purity metal is very sensitive to the amount of trace elements in it, especially at low temperature. As a consequence of this, the RRR test emerges as an extremely sensitive qualitative method of measuring purities of 99.999% and higher [30].

The resistance is the property of materials by which they oppose the passage of electrons through them. According to the Matthiessen law, it can be expressed as:

$$\rho_{tot} = \rho_i + \rho_d + \rho_t \tag{4.8}$$

where ρ_i shows the dependence between resistivity and the level of impurities, ρ_d is resistivity due to extended defects in crystal structure such as dislocations and grain boundaries and ρ_t displays the influence of temperature in resistivity as a result of the scattering of electrons due to thermal vibrations in the lattice [26].

As the thermal contribution will almost vanish at sufficient low temperatures, it is then easy to see that the responsibles for the residual resistivity are defects and impurities. Thus, to quantify accurately the influence of impurities and measure precisely the value of RRR the effects of ρ_d need to be minimized. For well-annealed metals with the highest purity, the contribution of ρ_d is small

compared with that of ρ_i [30] so the RRR is a good measure of the contribution of ρ_i.

Caution should be taken when using RRR as a characterization of purity mainly for two reasons. The first one is that only atoms in solid solution scatter effectively electrons, so nothing can be said about the impurity content in precipitate form. Additionally, RRR becomes a sensitive measure when the impurity level is about 100 ppm or less [30].

In the production of Superconducting Radio Frequency (SCRF) cavities, RRR is an essential value because of its relation with the grade of purity of the material (what is an indicator of the feasibility of reaching the desired accelerating gradients) and also because its relation with thermal conductivity, another necessary attribute of the materials for SCRF cavities.

Accelerating gradients

A large number of mechanisms are involved in the gradient limitation of SCRF cavities, and thus, its performance will be limited by whatever mechanism produces the lowest gradient limitation. Among the most important ones we find the quench magnetic field, with a critical value of around 240 mT, which has been thought to be an ultimate limit [6]. But there are other mechanisms involved in the gradient limitation, from which two of them should be highlighted in this text because of their relation with impurities and hence RRR.

The first one is field emission (FE), which produces emission current and radiation with the consequent undesirable beam loading. The sources of FE are impurities in the surface and sharp tips on the surface of the cavity. They can be removed with electropolishing and high pressure water rinsing (HPWR) [6].

The second one is thermal breakdown, caused by defects and/or impurities in the material's surface that create hot spots (thermal dissipation by ohmic effect) which locally enhance magnetic fields. At certain frequencies, it can be even more limiting than the quench magnetic field [6].

Thermal conductivity

In view of the fact that free electrons are the responsibles of electric and thermal conduction in pure metals, it might exist a correlation between these two param-

eters. Wiedemann and Franz (1853) proposed an inversely proportional relation between thermal conductivity and electrical resistivity [26]. This implies that high RRR values involve high thermal conductivity, what is very desirable in the design of SCRF cavities. The reason for this is that any kind of accidental heating could be quickly evacuated to the liquid Helium bath. Thus, high thermal conductivity stabilizes against breakdown at normal conducting spots [6].

4.3. Electron Beam Welding

Electron Beam Welding (EBW) is a fusion welding process in which the joint to be welded is heated by bombarding it with a dense stream of high velocity electrons [31]. The kinetic energy of the electrons is changed into heat when it impinges with the workpiece.

The electron beam is produced in a high - vacuum environment by an electron gun, usually consisting of a cathode (tungsten or tantalum), a grid or forming electrode and an anode. Electrons are emitted from the cathode which is heated to temperatures about 2750°C [32]. The electrons are then accelerated to a high velocity and shaped into a beam with the help of electrical fields. The beam is collimated and focused by passing through the field of electromagnetic focusing coils. Electron beams can be deflected from their normal path by magnetic deflection coils, usually located bellow the focusing coil. An schematic representation of an EBW device can be seen in Figure 4.10.

The gun is held at a high vacuum ($10^{-}4$ to $10^{-}5$ torr or less) to protect the cathode from oxidation and to ensure a proper insulation between the anode, the cathode and the control electrode [32]. The vacuum environment also reduces electron scattering by air molecules, thus conserving effective beam energy [31].

In the welding process, the beam first creates a hole in the workpiece. As the electron beam advances along the joint, a weld is formed by a combination of three effects that occur at the same time: 1) metal on the leading side of the hole vaporizes and then condenses to form a molten metal on the trailing side of the hole; 2) the molten metal on the leading side of the hole flows to the trailing side of the hole; and 3) the molten metal formed this way continuously fills the hole and solidifies as the electron beam advances [31].

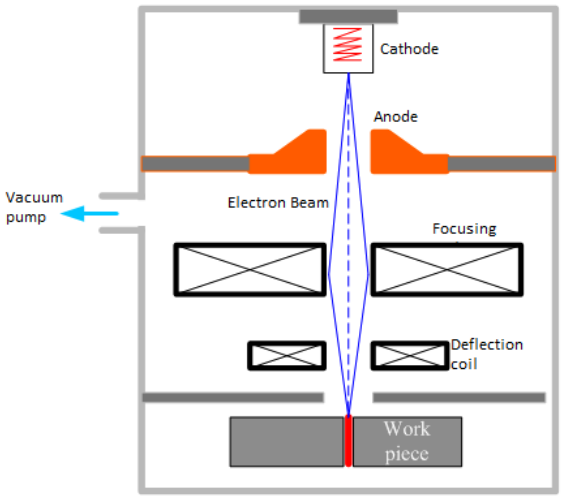

Figure 4.10.: Schematic of a conventional EBW device

Difficulties of Welding Dissimilar Materials

One of the main requirements for reliable welding is a knowledge of the properties of the materials and how they are affected by the thermal processes taking place. In most cases, whether or not a material is suited to a welding and to what extent its mechanical properties might be affected depend on a great number of factors so based only in general information is rather difficult or not even possible to predict. According to DIN 8528 Part 1, the weldability of a component is determined equally by its suitability for welding and the welding processes to be employed during its manufacture. Whether or not a material is suitable for welding can initially be determined by testing the characteristic properties and mechanical strength after welding [32].

But even when the respective weldabilities of two different materials are known, how they will behave when welded together still cannot be predicted. Not only their differences in physical properties such as melting point and coefficients of thermal conductivity play an important role, but also the metallurgical behavior of both parent metals acting as a binary alloy in the fusion zone [32]. The main difficulty with molten mixtures from the point of view of weldability if the formation of highly brittle intermetallic phases.

5. Experimental and Results

This chapter gives details of the experiments conducted for the purposes of the present study and the results obtained. In a first part, a description of the materials utilized and their preparation steps is presented. The second part, contains the characterization of the main properties of niobium and the effect of welding in the RRR value. The last part of the chapter contains the study of the dissimilar niobium–Ti6Al4V weld.

5.1. Materials

For the present work, the materials that were used were high purity niobium and a titanium alloy (Ti6Al4V). Their main physical characteristics and some others interesting for the application in which they will be used are summarized in Table 5.1.

Characteristic	Niobium	Ti6Al4V
UTS / (MPa)	199±2.4	1145±8.4
$R_p0.2$ / (MPa)	83±5.7	1188±34.3
A / (%)	25.7±6.64	9.8±0.90
Density/(g·cm^{-3})	8.6 - 8.7	4.4
Melting temperature/(°C)	2460 - 2470	1610 - 1660
Thermal conductivity/(W·m^{-1}·°C^{-1})	54 - 57	7.1 - 7.3
Cp/(J·Kg^{-1}·°C^{-1})	260 - 275	528 - 548

Table 5.1.: Physical characteristics of Niobium and Ti6Al4V. Mechanical properties (UTS, $R_p0.2$ and A%) were measured in the actual material used for the experiments while the rest of them come from [11]

5.1.1. Sample preparation

Pure niobium is soft and ductile and any loose or fracture abrasive particles can easily embed in it. This makes specimen preparation very difficult because it gums up diamond grinding disks or becomes embedded with fractured SiC particles when ground with SiC papers. This embedded particles may cause problems during the polishing and finishing steps.

For this reason, very careful handling of the samples is required to achieve mirror - like finishing. The steps followed for the preparation of the niobium samples were:

- **Mounting:** compression mounting with polymeric resin.
- **Grinding:** the grinding process started with a 80 grit SiC abrasive paper water cooled until the sample was flat and the effects of the prior operations were removed. The next paper should remove the effects of the prior paper in a short time, so the sequence followed was 80, 180, 240, 320, 600, 1200 grit abrasive papers.
- **Polishing (I):** When the sample was flat, a hard woven cloth with a 9 μm diamond suspension was used for around 10 minutes.
- **Polishing (II):** After this, a medium hard synthetic silk cloth with a 3 μm diamond suspension was used for 8 minutes time.
- **Finishing:** The last polishing step (also known as finishing) was carried out with a soft, porous and chemically resistant synthetic cloth sprayed with a mixture of 1 part of H_2O_2 (30%) to 5 parts of 0.05 μm colloidal silica for 5 minutes.
- **Etching:** Following ASTM E407–93 standard, etchant solution 160 was used mainly for grain revealing.

For more detailed information about niobium's preparation including the exact cloths used, force and speed of the automatic polishing device go to Appendix A.

For the preparation of the samples containing both niobium and titanium, the same mechanical preparation as for pure niobium was followed based on the

experience which shows that, when the sample is composed of different elements with different properties, the preparation to be followed must be the one of the most delicate element.

But for the final step, as the samples are composed of two different metals, the etchant solutions proposed in ASTM E 407–93 did not provide an homogeneous etching. A new solution was created based on the above mentioned standard. The etching procedure consists in immersing for 75 seconds the sample on an acid mixture containing 5 parts of H_2O, 6 parts of HNO_3 (65%) and 1 part of HF (48%) in volume. Better results specially concerning the Titanium grains are achieved with an aged etching solution.

5.2. Niobium

A prototype niobium plate was provided by PLANSEE. The piece (Figure 5.1) was an on-the-shelf scrap that, according to the supplier, was representative of the quality they can achieve.

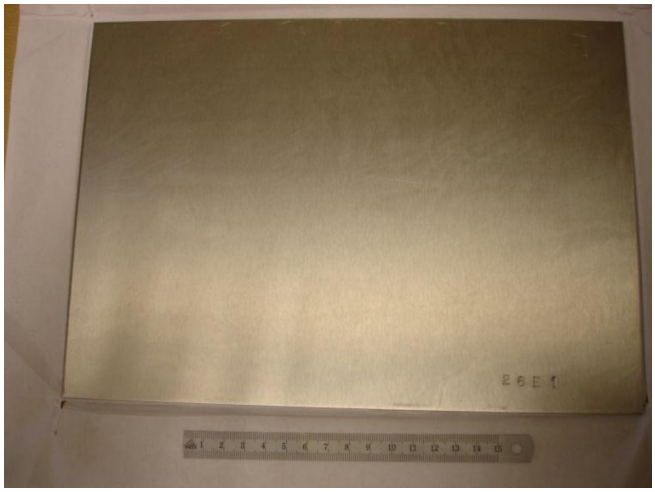

Figure 5.1.: Niobium test piece for qualification as delivered

To assess the effect on the degradation of the RRR values when submitted to EB welding, another niobium plate of the same quality also provided by PLANSEE was used.

5.2.1. Niobium raw material qualification

The properties tested were:

- **Ultrasonic inspection**, for continuity faults and for variations of attenuation
- **Surface roughness**, Rt
- **Tensile properties**, longitudinal and transverse to rolling direction
- **Microstructure**, for grain size and uniformity
- **Hardness**, HV10
- **Electrical RRR**, in bulk material both longitudinal and transverse direction

Ultrasonic inspection

The piece was US controlled immersed in demineralised water with the beam perpendicular to the surface using a Krautkramer USN 60 digital signal processor with a Da 201 probe of the same brand at 5 MHz (Figure 5.2). The whole piece was scanned according to specification CERN 3300 Ed. 2 - 20.07.2011. No discontinuities were detected and attenuation variation was lower than 20%.

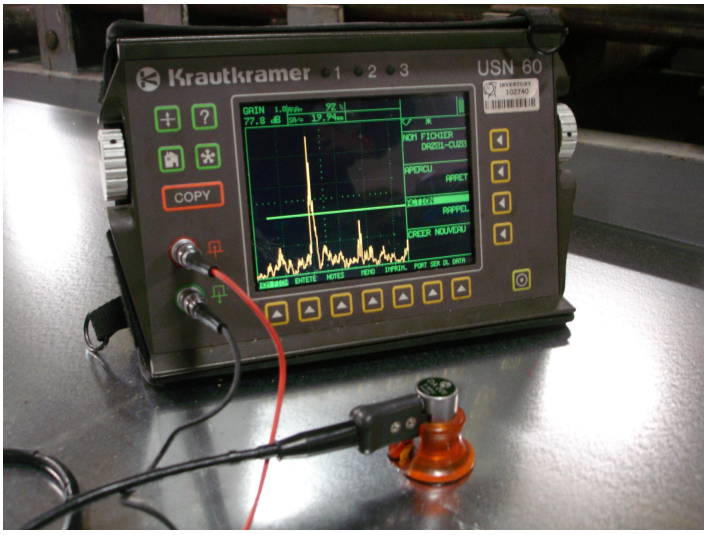

Figure 5.2.: US testing digital signal processor and probe

Surface roughness

The piece was controlled at six locations on every side along 4 mm lengths perpendicular to rolling direction using a Mitutoyo SJ-301 skid probe SR60 (Figure 5.3) and a Gaussian filter.

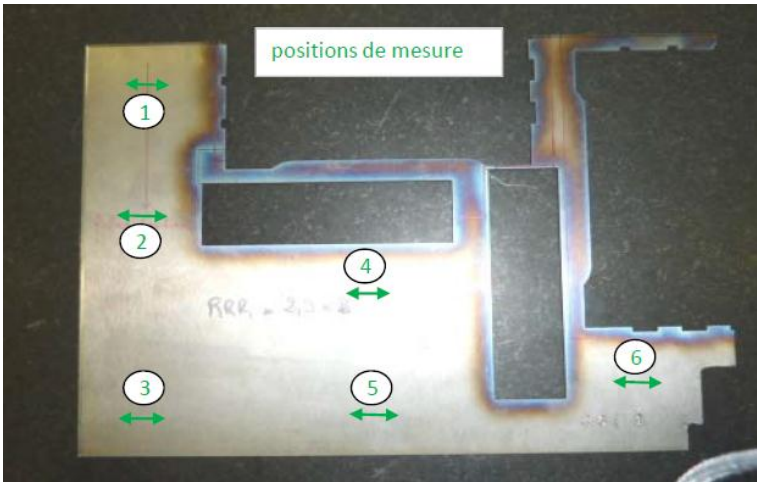

Figure 5.3.: Sample plate with the positions of the roughness measurements

Ra and Rt were evaluated according to ISO 4287:1997 and values are shown in Table 5.2:

Roughness measurements			
Face A		Face B	
Ra/(μm)	Rt/(μm)	Ra/(μm)	Rt/(μm)
0.98	8.57	1.12	8.59
0.87	10.25	1.38	13.34
0.94	11.00	1.34	12.38
0.99	11.04	1.16	11.62
0.95	9.15	1.25	14.15
0.94	8.34	1.37	17.43

Table 5.2.: Roughness measurements carried out in both faces of the sample plate

Tensile tests

Tensile tests were performed on two samples extracted by Electrical Discharge Machining (EDM) from the rolling direction and three samples extracted from the transverse direction with the help of a UTS 200 tensile machine (Figure 5.4) equipped with an extensometer whose resolution is higher than 0.4 mm. The stress rate in the elastic range was set to 5 MPa/s and the strain rate in the plastic range to 0.1 %/s.

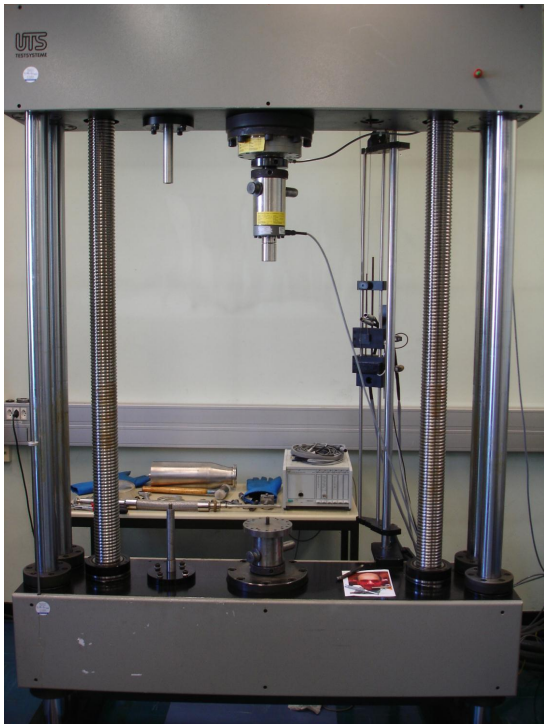

Figure 5.4.: UTS 200 tensile machine

The results of the tests are presented in Table 5.3. The average tensile strength in the rolling direction was 197±2.0 MPa and in the transverse direction was 200±2.7 MPa. The average yield strengths in the rolling and transverse directions were 76±0.8 MPa and 88±2.2 MPa respectively. The average tensile elongations at break in the rolling and transverse directions were 36±4.9% and 29±0.8% respectively.

Transverse direction			Rolling direction		
UTS/(MPa)	Rp0.2/(MPa)	A/(%)	UTS/(MPa)	Rp0.2/(MPa)	A/(%)
201	89	29.3	196	76	33.0
197	88	28.0	199	77	38.7
203	85	28.9	–	–	–

Table 5.3.: Results of the tensile tests in both longitudinal and transversal directions

Microstructure

For the microstructural observations, a Leica DM–RME optical microscope was used (Figure 5.5).

Figure 5.5.: Optical microscope Leica DM–RME

A 20 mm long metallographic sample of the cross section of the original 2.8 x 202 x 284 mm Nb sheet was cut parallel to what it was considered the direction of the last rolling operation. The samples were then prepared as explained in 5.1.1.

Micro-optical observations revealed heterogeneous grain size across the thickness of the plate (Figure 5.6a). It can be seen that in both upper and lower faces, the grain is fine and equiaxied (Figure 5.6b and Figure 5.6d), while in the central part, grains are coarser and elongated (Figure 5.6c).

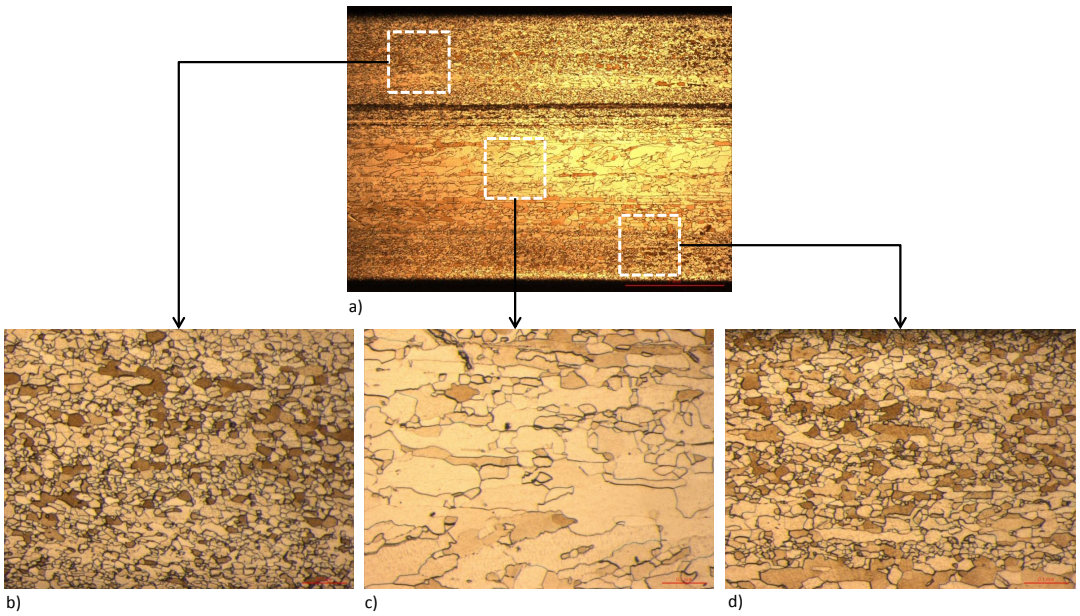

Figure 5.6.: Microstructural observations, showing detailed the top, central and bottom parts

The grain size in the region of equiaxied grains was measured according to the linear intercept procedure of ASTM E 112. A grains size number of G = 8.5 was found. This index corresponds to an average grain size diameter of 18.9 μm. In the region of elongated grains, grains up to 200 μm long were found.

Hardness measurements

HV10 hardness measurements were performed according to ISO 6507-1 using a Wolpert 2RC device. Three hardness measurements were done in each of the four corners of the plate as delivered. Additionally, four sets of three measurements each were carried out at random places of the surface of the plate.The average hardness results in 45.3 HV10.

RRR measurements for qualification

The measurement of the electrical resistances of the sample wires is based on the measurement of their voltage vs current curves (UI-curves). The samples are fixed in a window frame fiberglass holder (130 x 100 mm) and connected in series (Figure 5.7). While the current is ramping up step by step through the

samples, the voltage drop on each sample is measured. The electrical resistances are calculated by a least square fit of the obtained UI-curves. The temperature is verified by a calibrated carbon-ceramic resistor fixed close to the reference wire. During the tests the holder is always in horizontal position to minimize the thermal non uniformity along the samples [33].

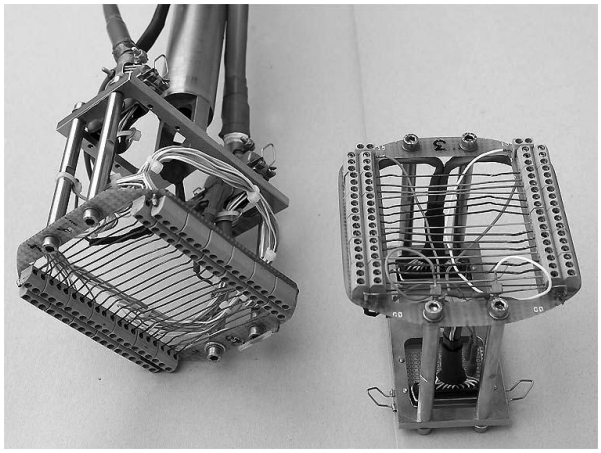

Figure 5.7.: RRR sample holders

The resistance at low temperature is measured by warming up the samples inside the cryostat from 4.2 K to a temperature just above the superconductor critical temperature. This condition is achieved by turning on the heater installed on an intermediate vertical tube (Figure 5.8) to heat up the helium gas around the samples.

For the data acquisition, the instruments used were a nanovoltmeter KEITHLEY2182 and voltmeters KEITHLEY2001 and KEITHLEY2000. All the communications between the workstation and the data acquisition instruments are performed by means of an ANSI/IEEE-488.2(GPIB) bus. The instruments were controlled by a LabVIEW based program.

Five samples 2 x 2 x 100 mm were extracted from the rolling direction and another five with the same dimensions were extracted from the longitudinal direction by (EDM) and milling. They were etched in an acid mixture of HF, HNO_3 and H_3PO_4 during 100 min in order to remove any contaminated and cold worked cortical layer. For the samples parallel to the longitudinal direction, the initial temperature of the bath was 13 °C and the final temperature was 14.3 °C. For the samples parallel to the rolling direction, the initial temperature

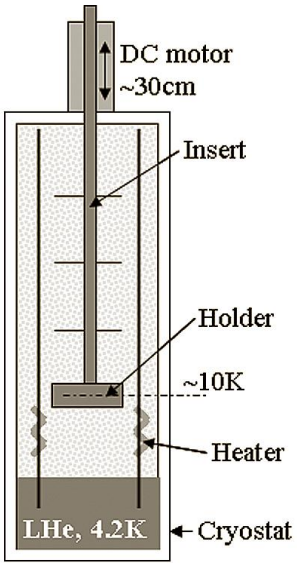

Figure 5.8.: Schematic of a RRR station [33]

was 11 °C, with a final temperature after the treatment of 12.8 °C.

The resistivity of the etched samples was measured at room (293 K) and at cryogenic (9.3 K) temperature. The RRR value in the longitudinal direction was 197±1 and in the transverse direction was 192±1.

As this RRR values seemed too low and in order to get free from any possible cold work that could have been induced by milling and not removed by the etching, two new samples 2.8 x 2.8 x 100 mm were extracted by EDM only; one parallel to the rolling direction and one to the transverse direction. They were etched twice in the same acid mixture mentioned above during 100 minutes each time. Initial and final temperatures of the bath were 9.4 °C and 12.3 °C respectively.

The resistivity was measured at room (293 K) and at cryogenic (9.4 K) temperature. The RRR values obtained were 183 for the transverse direction sample and 186 for the longitudinal direction sample.

5.2.2. Effect of EB welding on the degradation of the RRR values

All the welding processes carried out in this work were done in a PTR welding machine described in Table 5.4.

Maximum power/(kW)	30
Maximum voltage/(kV)	70
Maximum intensity on the filament/(mA)	420
Gun position	vertical
Chamber vacuum/(mbar)	$4{\cdot}10^{-4}$
Chamber length/(m)	5
Chamber diameter/ (m)	1.4

Table 5.4.: Characteristics of PTR welding machine

Two electron beam welding butt joints were developed perpendicularly to the last rolling direction on a RRR300 quality niobium provided by Plansee. In the first one (welding A), the material was only degreased before the welding process. In the second one (welding B), the material was also etched prior to the welding process with an acid mixture of HF, HNO_3 and H_3PO_4.

Six 2 x 2 x 100 mm samples from each weld were extracted parallel to the direction of the weld by EDM and milling at different distances from the weld axis according to the scheme shown in Figure 5.9.

Also five reference samples of the same size were extracted prior to the welding process parallel to the direction of the last rolling (perpendicular to the weld bead) and from a different location than the weld.

After the extraction of the samples, they were degreased and etched in an acid mixture of HF, HNO_3 and H_3PO_4 in order to remove any contaminated and cold worked cortical layer. For weld A, the samples were held from their top part and placed vertically in the bath. This made the section of the samples become non homogeneous as it can be observed in Figure 5.10.

To avoid the variation of section, a support was designed and built in polytetraflouroethylene to keep the samples horizontally in the etchant bath (Figure 5.11).

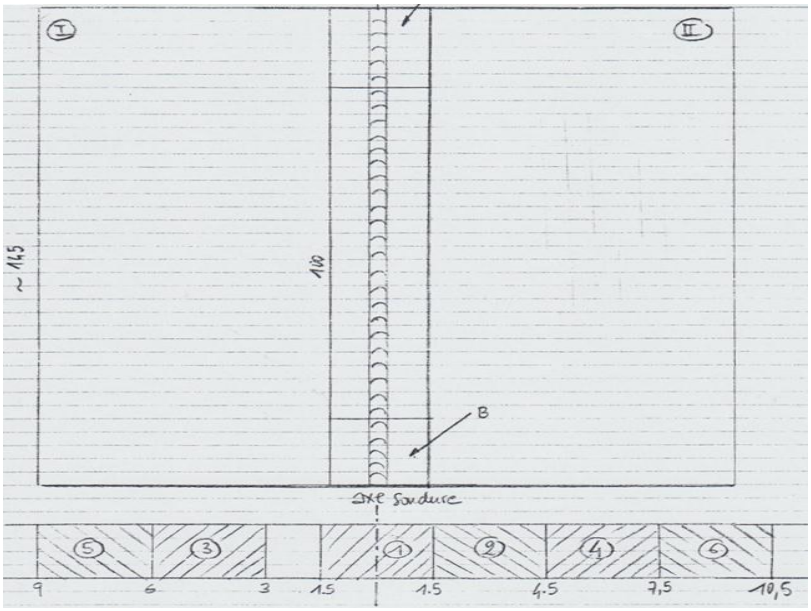

Figure 5.9.: Schematic drawing of the position of the samples for RRR measurements with the relative distances in millimeters of the samples to the weld bead

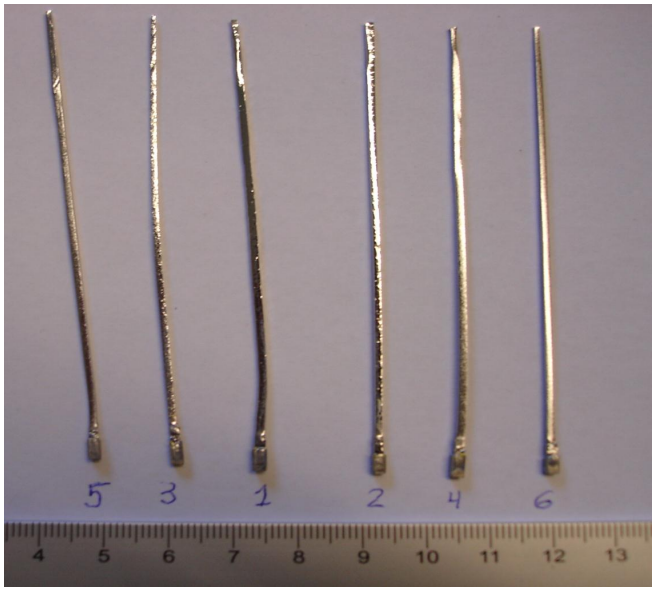

Figure 5.10.: Aspect of samples 1 to 6 of welding A after chemical etching

The selection of the material was based on its polymeric nature and its density, higher than the acid mixture to avoid the holder to float in the bath.

In Figure 5.12, it can be seen the different values of the RRR parameter

Figure 5.11.: Support to keep samples horizontally in the chemical etching bath

depending on the distance from the weld bead just after the transition temperature. The unfilled points correspond to the reference samples.

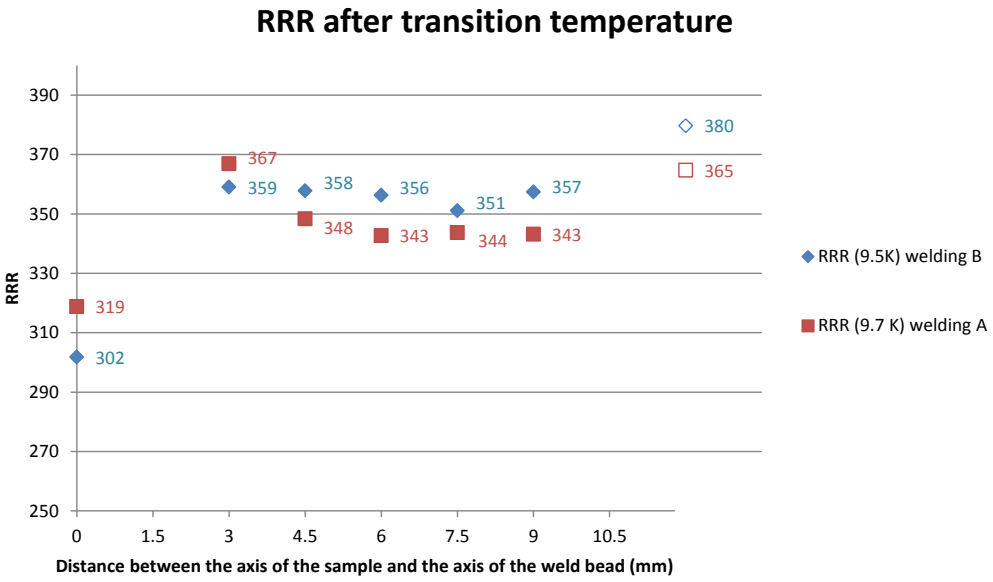

Figure 5.12.: RRR values depending the distance from the weld bead after transition temperature

5.3. Niobium–Ti6Al4V weld

The test materials were high purity (RRR $\geq$ 300) niobium produced by Plansee and a Ti6Al4V sheet. The niobium plate was 3 mm thick and the 3.5 mm thick titanium plate was milled so that the two materials had the same initial thickness. Additionally, influence of heat treatment (HT) (800°C - 2 hours) on the quality of the weld was studied.

Testing program was inspired by ISO 15614-11 but toughness tests were not done as the thickness of the samples was not enough according to ASTM A370. The following tests were carried out:

- Penetrant liquid test
- Radiographic examination
- Macrostructural observation
- EDS analyses for composition
- Transverse tensile tests
- Microstructural observations
- Hardness tests
- XRD

After NDT, four tensile samples were cut perpendicular to the direction of the weld. The remaining cuttings were used for microstructural assessment, hardness profiles and EDS analysis. Table 5.5 summarizes the different tests carried out in the different samples.

It also shows which samples were submitted to heat treatment and which were not. With the aim of having more statistical data, samples B and D were cut in two parts to which we will refer as left (L) and right (R).

Before starting with the heterogeneous joint, Nb/Nb and Ti/Ti welds were carried out in order to have starting point parameters. Additionally, as a result of the great differences in physical characteristics shown in Table 5.1, special settings were used in order to achieve a good quality weld. These parameters are given in Table 5.6.

Sample	HT	NDT	DT
A	No	Yes	–
B	Yes	Yes	EDS, μstructure, hardness
C	No	Yes	EDS, μstructure, hardness
D	No	Yes	EDS, μstructure, hardness
E	Yes	Yes	EDS, μstructure, hardness
1	No	Yes	Tensile test, XRD
2	No	Yes	Tensile test
3	Yes	Yes	Tensile test
4	Yes	Yes	Tensile test

Table 5.5.: Description of the samples and of the tests carried out on them

Dye penetrant inspection

DPI was carried out over the whole surface of the weld and on both sides according to EN 571-1 :1997.

The weld presented no indication, i.e. non evolutive surface defects are observed after 20 minutes of developing.

X–rays

The whole weld was controlled according to EN 1435 B using a Phillips MG161L + MCN166 X–Ray tube and two 0.027 mm Pb screens per film with an accelerating voltage of 100 kV. Due to the great difference in density of the two base materials, a multifilm method was used. This method consists in irradiating simultaneously a combination of films with different sensitivities so that an 'average' effect is achieved while observing them superimposed. By means of this technique, a good resolution in the weld bead was obtained as it is seen in Figure 5.13.

The evaluation resulted conform according to the BN ES ISO 13919-2:2001 with CERN restrictions EN ISO 6520 acceptance criteria. Only a small dark spot that could have been a discontinuity was found, but this possibility was discarded after metallographic observation of the cross section.

Welding speed/(mm·s^{-1})	12
Distance from gun to work/(mm)	350
Beam deflection/(mm)	0.65
Oscillation frequency/(Hz)	200
Beam acceleration voltage/(kV)	60
Beam current/(mA)	30
Focusing current/(mA)	
-First coil	1000
-Second coil	420
Focal plane	on top of the surface
Beam position	shifted towards Nb side

Table 5.6.: Welding parameters

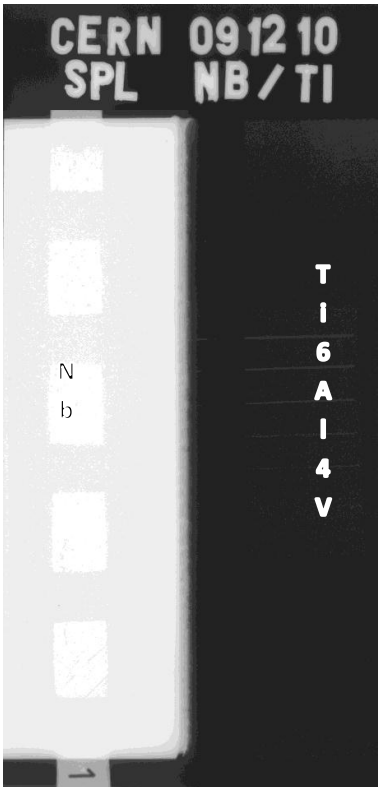

Figure 5.13.: X-ray radiography of the weld showing niobium on the left (bright) and titanium on the right (dark)

Macroanalysis

Macrographies of the cross sections of the weld were carried out with a Sigma ZEISS scanning electron microscope (SEM) shown in Figure 5.14. This microscope is fitted with a high current column upgrade delivered with an extra large aperture of 240 μm giving a maximum current of 40 nA. The main parameters of the microscope are presented in Table 5.7.

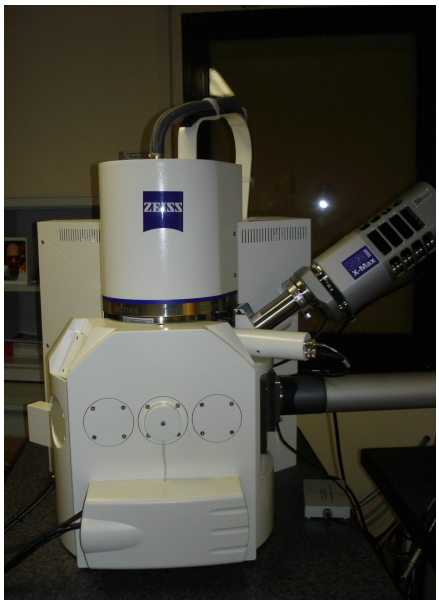

Figure 5.14.: SEM Sigma from Zeiss

Resolution/(nm)	1.5@ 20kV and WD = 2 mm
Magnification	500000x in SE mode
Electron source	Schottky thermal field emitter
Accelerating voltage/(kV)	0.1 - 30 kV
Probe current/(pA)	4 - 40000

Table 5.7.: Main parameters of the Sigma SEM

Single pictures were taken at 200x magnification and then an overall image was reconstructed with the help of a multiscan tool. Backscattered electron detector was used as it is more sensitive to the atomic number of the present elements and thus, to the composition of the sample.

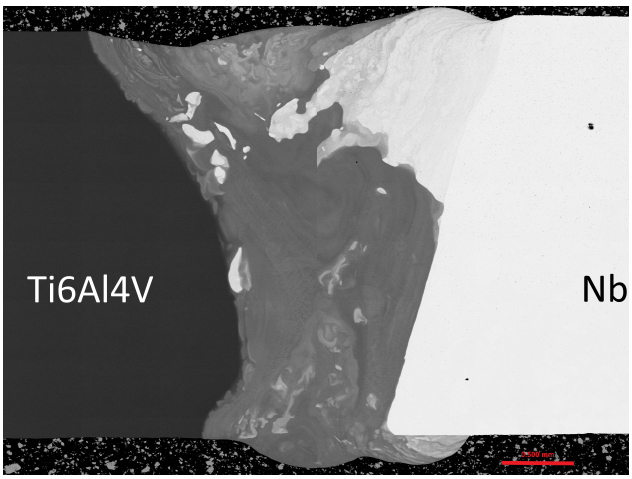

Figure 5.15.: Macrograph of weld (Sample D (L)). Backscattered electron image of the overall aspect of the cross section of the weld.

It can be seen in Figure 5.15 a big heterogeneity on the upper part of the niobium side apparently rich in this element. A more careful observation shows a small overlap in the root of the niobium side. No remarkable differences regarding the morphology of the weld were observed after heat treatment.

EDS analyses

EDS semi–quantitative analyses were performed in the cross sections of samples C and D before HT and on samples B and E after HT in order to asses the composition of the bead. The device utilized was a Sigma ZEISS scanning electron microscope equipped with a 50 mm^2 Oxford Instruments detector and supported by INCA software for the EDS analyses.

A representative cross section before HT and another one after HT are presented in Figure 5.16 and Figure 5.17 respectively, where EDS semi–quantitative maps of Ti and Nb can be observed. Although V and Al are present as alloy elements in the Ti6Al4V, EDS analyses showed that they were homogeneously distributed in the same places where Ti was found so their maps are not included in this work as they do not provide any additional information.

Regarding the samples before HT, the analyses show a bead rich in Ti as it can be interpreted from Figure 5.16. The bottom half shows a homogeneous dilution between the materials with around 70% in weight of titanium. There

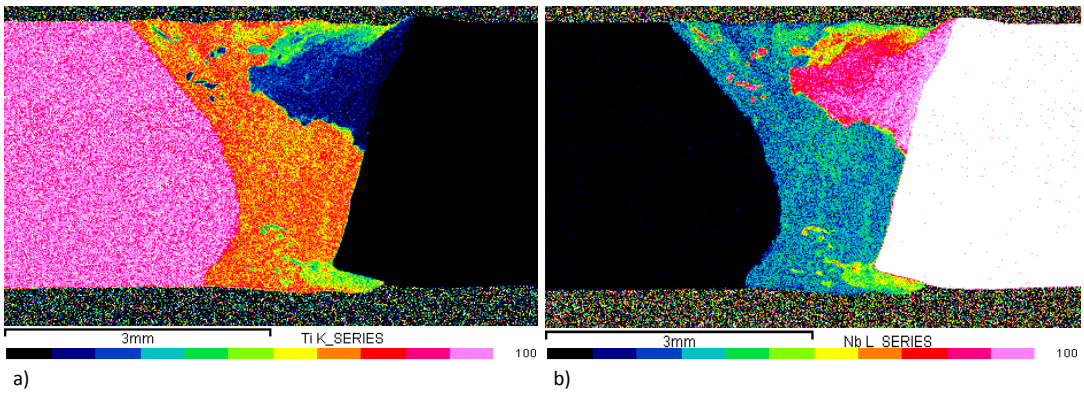

Figure 5.16.: EDS quantitative maps of sample D(R). Figure 5.16.a) represents the weight percentage of Ti. Figure 5.16.b) represents the weight percentage of Nb.

is also a small area at the root of the niobium side with around 50% in weight of niobium. The top half of the bead is less uniform. A big Nb heterogeneity can be observed on top of the Nb side containing around 90% in weight of this element. Small Nb islands appear at random places of the top part of the weld bead.

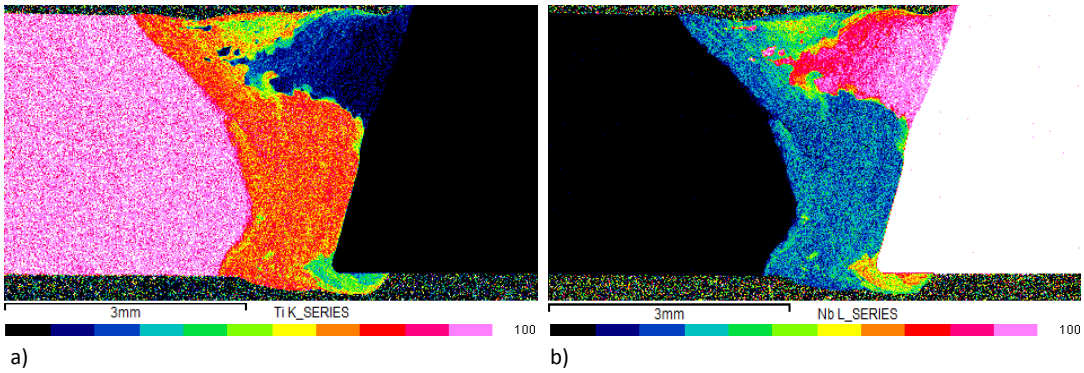

Figure 5.17.: EDS quantitative maps of sample E. Figure 5.17.a) represents the weight percentage of Ti. Figure 5.17.b) represents the weight percentage of Nb.

For the samples after HT, there is no remarkable difference in terms of composition as it can be seen in Figure 5.17. The bead's composition is still being around 70% in weight Ti and the same inhomogeneities as before HT are observed. The only change observed is that, in the root of the Nb side, it can be

seen a small overlap.

Tensile tests

Tensile tests were performed on four samples extracted transverse to the welded joint with the weld bead in the middle of the calibrated length. The geometry of the samples was designed in accordance to EN 10002 as shown in Figure 5.18. All samples were tested with the help of a UTS machine equipped with an extensometer described in 5.2.1. The stress rate in the elastic range was set to 10 MPa/s and the strain rate in the plastic range to 0.1 %/s. Samples 1 and 2 were tested before HT and samples 3 and 4 after HT.

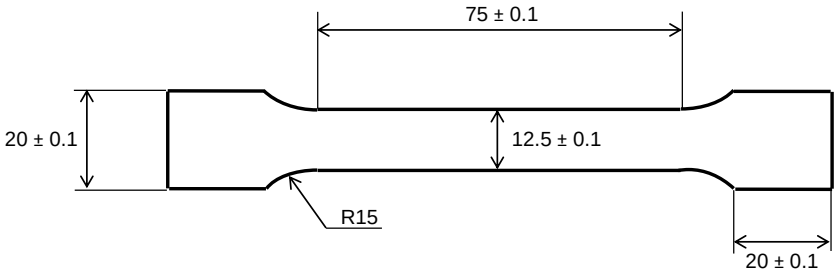

Figure 5.18.: Tensile specimen

The strain - stress curves as well as a summary of the most relevant results are shown in Figure 5.19 and Table 5.8 respectively. For the elongation at break after HT, the variation of length (Δl) was calculated by measuring the length of the sample before and after the test. The reason for this is that it is a much more accurate method when the break occurs outside the extensometer. For this reason the values of this parameter do not match with the ones shown in the curve.

	Before HT	After HT
Tensile strength/(MPa)	153±2.7	159±2.2
Elongation at break/(%)	24.8±2.70	26.6±0.10
Failure location	Bulk niobium	Bulk niobium

Table 5.8.: Summary of tensile tests results

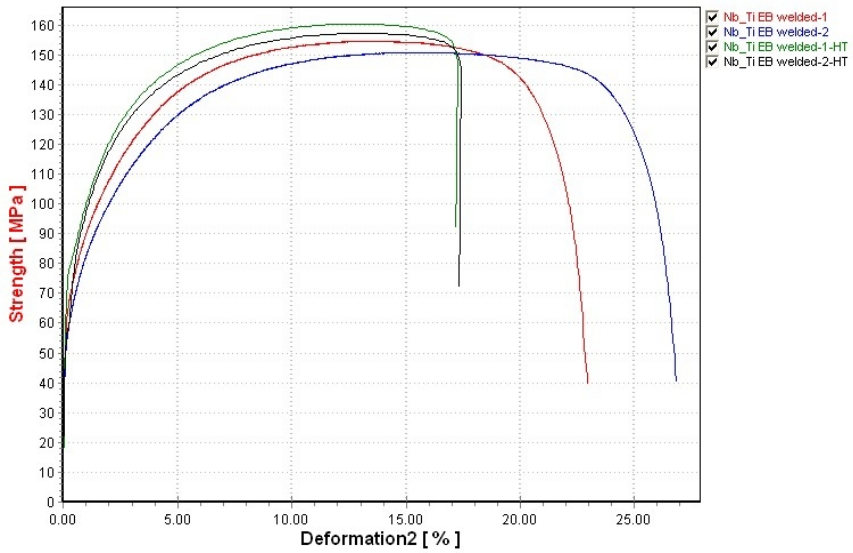

Figure 5.19.: Stress - strain curves of the samples before and after HT

Metallography

For the microstructural observations, a Keyence VHX1000 digital microscope was used (Figure 5.20). It is a variation of a traditional optical microscope that uses both optics and electronics, coupled to a camera to output a digital image to a monitor.

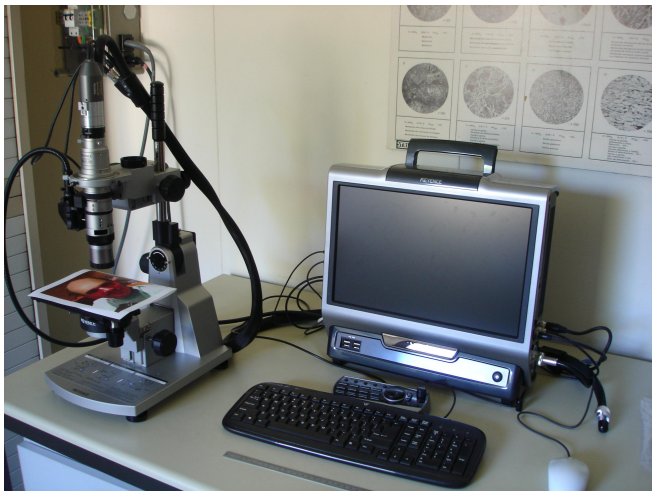

Figure 5.20.: Digital microscope KEYENCE VXH1000

Samples from the cross section of the weld bead before and after HT were prepared as explained in 5.1.1. A representative section of the weld can be

observed in Figure 5.21.

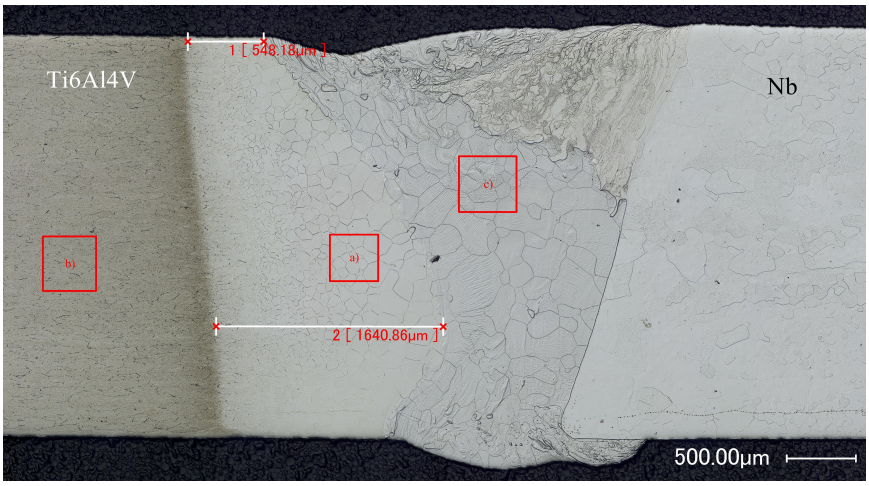

Figure 5.21.: Metallography of the weld (Sample D (L))

It can be seen very clearly the Heat Affected Zone (HAZ) on the titanium side with a minimum width of 548 μm and a maximum of 1641 μm. The microstructure of this recrystallized zone observed in Figure 5.22.a is a Widmanstatten ($\alpha + \beta$) structure as it is explained in [34]. It is also very characteristic the typical ($\alpha + \beta$) structure observed in the titanium side outside the HAZ, with equiaxied α (bright) and small amounts of intergranular β (dark) (Figure 5.22.b). It is not so evident, if it exists, the HAZ of the niobium side. Regarding the weld bead, it is observed a typical solidified structure. The patterns, are not confined inside the grains (Figure 5.22.c).

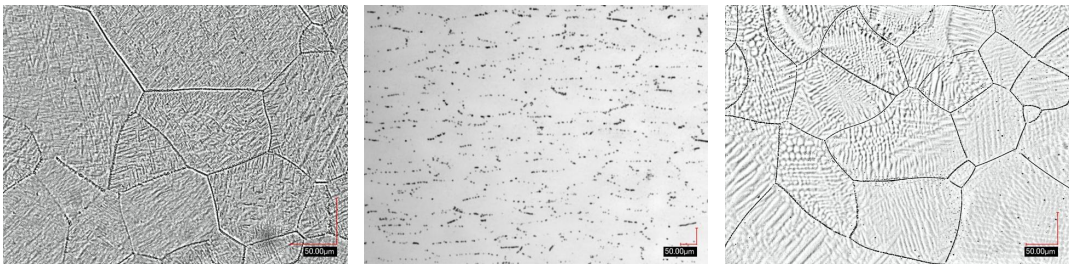

Figure 5.22.: Microstructures of sample D (L). Figure 5.22.a) represents the HAZ of the Ti6Al4V side. Figure 5.22.b) shows the microstructure of the Ti6Al4V base material. Figure 5.22.c) represents the microstructure observed in the weld bead.

Special attention was put regarding the overlap observed in the root of the niobium side. When observing the area with higher magnification (Figure 5.23), grain growth across the interface is detected, what enhances the bonding between the two parts.

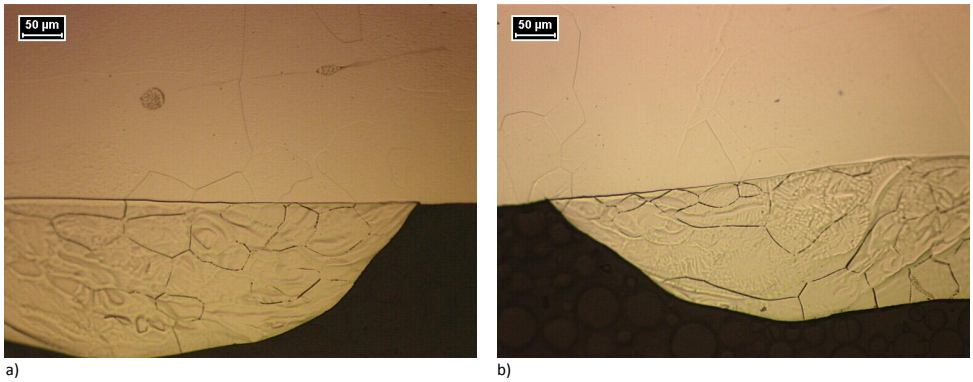

Figure 5.23.: Detail of the root of the niobium side

No substantial differences regarding microstructure are observed before and after HT.

Hardness

$HV_{0.05}$ measurements were performed on the cross sections of samples B, C, D and E using a Leitz microdurometer. Samples were prepared and etched, and microhardness profiles were carried out according to the 'rows of indentations' test procedure described in EN 1043-2.

A representative tested section is given in Figure 5.24. It can be observed that the hardness of the weld metal zone range from 201 to 311 $HV_{0.05}$, what is an intermediate value between the hardness of both parent metals. Also a slight hardening in the HAZ is detected. The hardness values measured in the niobium heterogeneity are not much lower than in the rest of the weld bead, and much higher than in the niobium side. Samples after HT did not show substantial differences in the hardness values compared to the samples before HT.

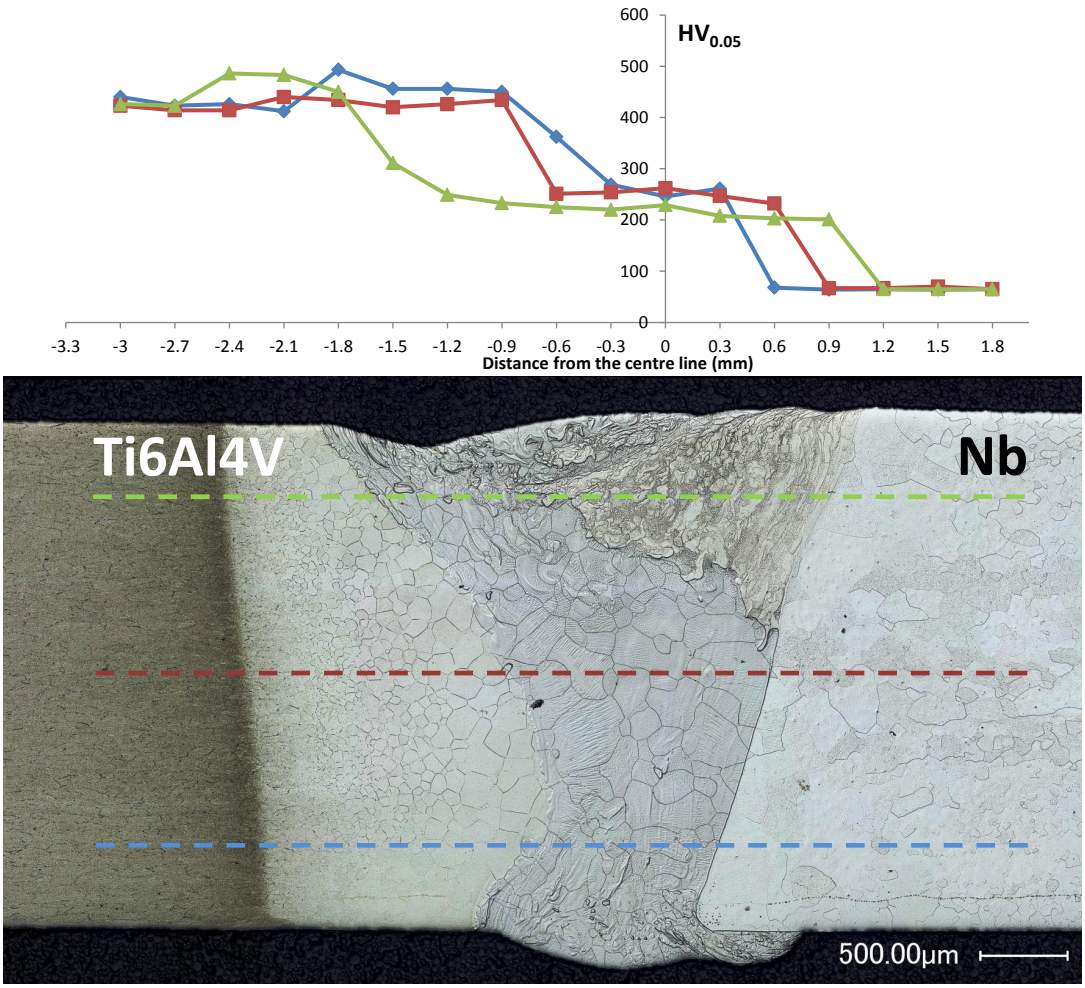

Figure 5.24.: Hardness profiles

X - Ray Diffraction

For the X–Ray Diffraction observations, a Cristalloflex D5000 from Siemens was used in the Bragg - Brentano configuration. The X–Ray tube and the detector aperture are on the common measuring circle, with the X–Ray tube mounted on the device.

A XRD spectrum was done in the weld bead of sample 1 in order to rule out the possibility of new phases have appeared after its solidification. For the acquisition, in order to scan only the weld bead, the apertures of the divergence slit, antiscatter slit and receiving slit were set to 0.2 degrees, 0.2 degrees and 1 mm respectively. With this configuration, the signal would have been very weak so to improve the quality of the spectrum, the step size was set to 0.02

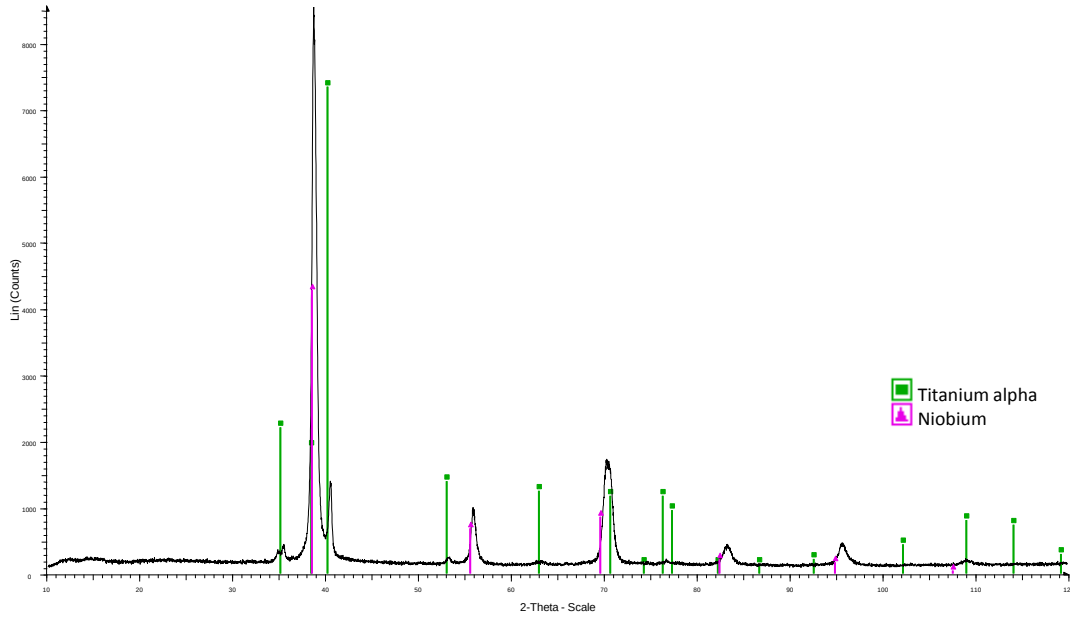

Figure 5.25.: XRD spectrum of the weld bead of sample 1 with the patterns of alpha titanium and niobium superimposed

degrees with a time per step of 8 seconds in continuous mode. The origin of the angles was set to 10 degrees, and the end was set to 120 degrees.

The obtained spectrum is depicted in Figure 5.25, as well as the diffraction patterns for titanium alpha and niobium. As it can be observed, all the peaks have been identified. It is also evident the shifting of the niobium peaks to the right with respect to the pattern.

6. Discussion

6.1. Niobium raw material

The results shown in 5.2.1 were compared to CERN 3300 Ed. 2 - 20.07.2011 technical specification titled *Sheets for superconducting applications: pure niobium RRR 300 grade*. This specification relates to pure niobium sheet RRR grade in fully annealed condition for superconducting applications at CERN requiring RRR minimum values of 300. Material shall conform to R04220-Type 5 as per ASTM B393-09e1 with additional and overriding requirements.

US inspection

The piece was found conform to the specification and to class 6 acceptance criteria according to standard prEN 4050 part 4. The fact that the attenuation is less than 20% means that the variation of the grain size along the sample it is not very high.

Surface roughness

Surface roughness can promote local normal conducting sites on the surface of a cavity which decreases its efficiency [35], reason why the surface roughness' constraints for the inner surface (RF surface) of the cavity are so restrictive.

For face A (written surface): Ra = 0.99 μm and Rt = 11.4 μm. That conforms to the specification of Rt $\leq$ 15 μm for the RF side and Rt $\leq$ 60 μm in the back surface.

For face B: Ra = 1.38 μm and Rt = 17.43 μm. That conforms to the specification of Rt $\leq$ 60 μm in the back surface but does not conform with the specification of Rt $\leq$ 15 μm for the RF side.

As there is only one RF side, the plate conforms to the specification as long as face B is defined as back surface.

Hardness

The average hardness results in 45.3 HV10. That conforms to the specification of maximum 60 HV10. The small dispersion of the results implies a high homogeneity.

Tensile tests

The specification requirements in terms of mechanical properties are oriented to guarantee that the formability of the niobium is enough to be formed by spinning or deep drawing to the final cavity geometry.

The average tensile strength in the rolling direction was 197±2.0 MPa, and in the transverse direction 200±2.7 MPa. This conforms to the specification of minimum 140 MPa.

The average yield strengths in the rolling and transverse directions were 76±0.8 MPa and 88±2.2 MPa respectively. This conforms to the specification of minimum 50 MPa and maximum 100 MPa.

The average tensile elongations at break in the rolling and transverse directions were 35.8±4.90% and 28.7±0.78% respectively. Only rolling direction conforms to the specification of minimum 30%, but transverse direction is very close to the specified value.

The relative difference in average values measured in longitudinal and transverse directions do not exceeds 20% as specified. This last condition infers that a high isotropy is found in the material, highly recomended for the accuracy needed in the forming processes that the plate undergoes.

Microstructure observation

The grain size number is 8.5 on the periphery, what corresponds to a 18.9 μm diameter. In the center, grains are up to 200 μm long. This is not in accordance with point 3.2.1 of the specification, requiring in first place 'structure completely recrystallized and uniform size equiaxied grains' and in second place grain size number of 5 or finer, being able to accept local values of 4.

An homogeneous microstructure with finer grain size is desirable to obtain good properties for forming and functioning in a high purity niobium cavity. A coarse microstructure leads to a rough surface or the so called orange peeling of the surface of the cavity [36]. In our case, the coarser microstructure is not on the surface, and the roughness values conform the specification.

The usual metallurgical procedures to control microstructure based upon second phases as centers of nucleation and growth may not be used for SC niobium. Such procedures would decrease the purity of the material, which is the most important parameter in SC niobium sheets. It is thus understandable the production challenge that involves such a high purity niobium in terms of grain size control, and the specification requirements might be on the edge of feasability.

For the reasons above explained and provided all the other parameters conform with the specification, fully recrystallized equiaxied grains with grain size number up to 4 (locally 3.5) could be accepted for the fabrication of SC accelerating cavities.

RRR measurement

RRR is an extremely sensitive qualitative method of measuring purities of 99.999% and higuer, required as the most important parameter for the fabrication of superconducting accelerator cavities for the reasons adressed in 4.2.7. As every manufacturing step can potencially decrease the RRR value, a very strict adherence to the specification is required for this parameter.

In a first measurement, the RRR values resulted to be less than 200, what is absolutely out of specification requiring minimum value of 300. A second measurement was carried out and the result resulted to be even lower. The difference between them can be ascribed to the extreme sensitivity of the RRR measurement to temperature. As the tests were done with a difference of 0.1 degree, a lower value appears in the 'hottest' test.

As far as regards the RRR value, no concession can be made so a sheet like this could never be accepted for the manufacturing of SC cavities.

6.2. Influence of EB welding in RRR values

The traditional fabrication techniques are based on deep drawing or spinning of the half cells and EBW of the equators and irises. Therefore, it is of paramount importance the effect that this joining technique has on the RRR value.

When comparing the values of the two welds, the difference between them is assigned to the different temperature at which the measurements where done. As resistivity increases with temperature, lower values of RRR appear in the samples from weld B, as they were measured at higher temperatures (9.7 K instead of 9.5 K for weld A). This also shows that the etching treatment before the welding process does not have much effect on the RRR value.

It is also evident a higher reduction of the RRR ratio in the sample situated on the weld bead compared to the rest of the samples. This is completely normal, as in the weld bead impurities from the surface might have been added to the material while it was in molten state. The rest of the samples were extracted from places where melting never occurred but a rise in temperature took place. This fact, together with the vacuum of the EBW machine might have helped to degas this samples. Nevertheless, the RRR value even in the worst scenario (Sample 1) is always above the specified value of minimum 300.

6.3. Weldability of niobium to Ti6Al4V via EB welding

The whole surface of the weld was tested via NDT and no defects were detected. This implies that, with the parameters described in Table 5.6, it can be achieved a weld that fulfills with the requirements demanded for the transitions of the cavity with the tank.

Macroscopic observations showed a wavy shape at the face of the weld, what can be ascribed to the oscillating movement of the beam during the welding process. An inhomogeneity was observed and was later studied in depth by means of EDS analyses, confirming that it was a volume rich in niobium. This volume probably solidified before it had time to mix with the rest of the bath as a consequence of the high thermal conductivity and high melting point of

niobium. The rest of the inhomogeneities observed in the bead were probably attached to the big niobium volume in a first moment. As a consequence of the energetic processes undergone by the bath during the welding process, they detached of it, solidifying before the rest of it due to the same reasons above explained.

From the EDS analyses and the tensile tests results, it can be inferred that the presence of heterogeneities in the bead does not affect the mechanical quality of the joint. The same statement can be done for the overlap observed in the root of the niobium side.

Hardness tests on the weld metal zone are of paramount importance because a rise in the hardness value would mean either that contaminating agents were present during the weld process or the presence of intermetallic brittle phases. According to the results, no rise on the values is observed so the cleaning of the pieces and the grade of vacuum is sufficient for the process. No intermetallic brittle phases were detected.

In the metallographic examination, HAZ on the titanium side is rather big for an EBW process, but the low thermal conductivity of Ti6Al4V alloy inhibits the heat flow so that a big recrystallized zone may appear. On the other hand, we have the opposite effect in the niobium side, whose high thermal conductivity enhances the heat flux. This combined with its higher recrystallization temperature makes this process very unlikely. Narrow weld bead is a typical feature of EB welding due to the low total heat input per unit length [37] so the metallography just confirms this broadly known fact. The microstructure of the Ti6Al4V base material, outside the HAZ is very typical of annealed $\alpha + \beta$ alloys [34]. The microstructure observed in the HAZ is also very common for titanium alloys heated above its beta transus temperature and then submitted to moderate colling rates as described in [34]. For the weld bead, dendrites coming from solidification are observed. To the already irregular solidification microstructure, it has to be added that the composition of the bead is mostly a mixture of titanium and niobium, so the etchant solution might have acted unevenly along its surface.

The root of the niobium side was studied in depth due to the overlap observed there. It is clear that in all the cases, a proper bonding is achieved. Even in the samples in which there is no apparent fusion of the parent metal, no detrimental

effects in the mechanical properties are detected due to the grain growth across the interface observed in Figure 5.23.

XRD spectrum showed no new phases in the weld bead apart from alpha titanium and niobium, as every peak has correspondence with one of the patterns. With respect to the shifting in the niobium peaks to higher angles, this could be explained by a smaller lattice parameter of the NbTi solid solution compared to the one of pure Nb. As in the weld bead we have a NbTi compound, M.Hansen et al. suggest in [38] a formula to calculate the variation of the lattice parameter with the relative composition of these two elements:

$$Nb_xTi_{1-x} \; for \; x = 0.25 - 1; \; a = 0.3273 - 0.3294 \; nm \tag{6.1}$$

From the EDS analyses performed, an average of 30% atomic of niobium is obtained, what gives a lattice parameter of 0.3274 nm. As the lattice parameter for Nb is a = 0.3294 nm, this corresponds to a shrinkage of 0.6%. When applying this correction to the niobium pattern, as it can be seen in Figure 6.1, it matches with the spectrum.

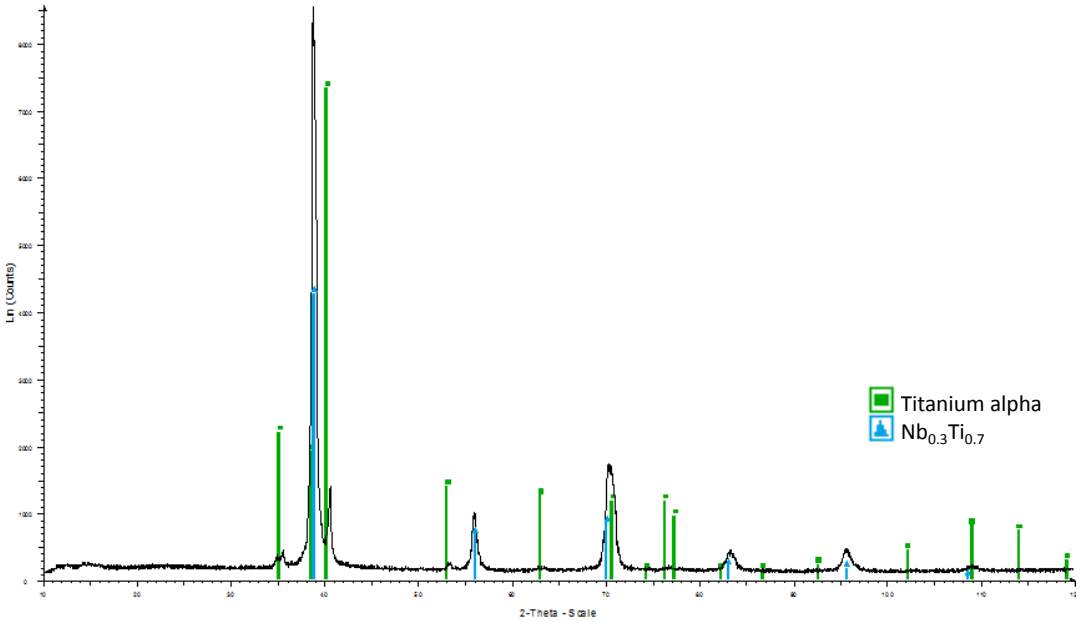

Figure 6.1.: XRD spectrum of the weld bead of sample 1 with the patterns of alpha titanium and $Nb_{0.3}Ti_{0.7}$ superimposed

6.4. Further work

In the following section, there can be found some suggestions of the continuation of the work already done. It is again divided in the three different subjects herein treated.

Niobium raw material

Regarding the niobium raw material, it has to be guaranteed by the supplier the feasability of a RRR $\geq$300 if required, and the values provided in their certificates should be double checked at CERN.

Weldability of niobium to Ti6Al4V

Heterogeneous zones observed in the weld bead need to be studied eventhough apparently do not affect to the quality of the weld. Further studies should be made in order to better understand the behavior of the bath during the welding process and thus find a new set of parameters that allow the material to mix and become more homogeneous.

It could also be very interesting to study the weldability of these two metals in a different geometry, more similar or identical to the one designed for the interfaces of the cavity and the helium tank as they involve much more welding difficulties.

Further studies suggest the use of a stainless steel tank instead of a Ti6Al4V mainly for economical reasons. In such case, two different solution for the interfaces can be considered:

- The conservative solution would do the transitions by means of a brazing between the niobium and SS, using oxygen free electronic (OFE) copper as filler metal.

- The most challenging one consists of a EBW between niobium and SS with a filler metal to be determined. Studies have started at CERN [4] inspired in the brazing procedure using also OFE copper, but intermetallic brittle phases with intolerably high hardness values were detected. A Cu - Ni alloy could be tried as filler metal.

7. Conclusions

From the results discussed in the present study, the conclusions that can be drawn are presented in this chapter.

7.1. Qualification of niobium raw material

- After the tests carried out on the sample plate, its quality is unacceptable as for CERN technical specification 3300 Ed. 2 - 20.07.2011 mainly because of its electrical properties (RRR $<$ 200). In previous samples from the same firm, RRR values were always higher than 300, and the material certificates demanded to them always showed values greater or around 300.
- The challenge that represents the grain size control in such a high purity material is understood as long as the US inspection is according to the specification. Grain size number smaller than 5 could be accepted.
- Surface roughness of Rt = 17.43 μm does not conform to CERN specification for the RF side, but an improvement of surface finishing and hence this value should be achieved with the chemical surface treatments to which the plate will be submitted.

7.2. Effect of EBW on RRR

- The reduction of the RRR value after a EBW process in the weld bead is less than 20% with respect its original value and, in both cases, the worst value remained over the RRR $>$ 300 threshhold. As a consequence, EBW under high vacuum is found to be a suitable process for the niobium interfaces of SCRF cavities.

- It is a standardized practice a slight etching before welding to remove oxides that could be detrimental for the welding process, but from a point of view of purity, the etching treatment undergone by the pieces before the welding process did not have much effect (if any) in the RRR value.

- There is a very important influence of temperature in the RRR value. Changes as subtle as 0.2 degrees drive to significant differences in the measurements. As a consequence, these test need to be carried out with extreme caution in order to have statistically significant data. Another possibility is measuring the RRR values at different temperatures so that the values can be extrapolated to 4.5 K.

7.3. Dissimilar EBW of high purity niobium to Ti6Al4V alloy: influence of heat treatment

- Based on the tests developed on a dissimilar joint of high purity Niobium and Ti6Al4V, electron beam welding seems to be a very suitable process in order to obtain joints that fulfill with the requirements demanded for the transitions of the cavity with the tank even in materials with such different physical properties. The absence of defects and the mechanical strength of the joint proves this fact.

- The heat treatment foreseen for the assembled component does not have any negative effect that degrades the quality of the weld. Moreover, the mechanical properties were improved after it and no signs of precipitation of intermetallic phases were observed.

- XRD and metallographic observations revealed no additional phases apart from the ones found in the parent metals.

- The heterogeneous zones observed in the weld bead do not affect the quality of the joint.

- It should be studied the feasability of the joint with different parameters that may drive to a more homogeneous weld bead.

Bibliography

[1] "http://www.cern.ch."

[2] R.Garoby, "Spl at cern," in *Proceedings of SRF 2009*, 2009.

[3] R. Garoby and M. Vretenar, "Cern/ps/rf," 1997. 96-27.

[4] O. Capatina, S. Atieh, I. A. Santillana, G. A. Izquierdo, S. Calatroni, A. DElia, R. Garoby, T. Junginger, D. Maciocha, E. Montesinos, V. Parma, T. Renaglia, T. Tardy, N. V. Alonso, and W. Weingarten, "Mechanical considerations for beta=1 cavities," in *SRF 2011*, 2011.

[5] C. Adolphsen, "International linear collider (ilc) linac basics," tech. rep., SLAC, 2006.

[6] N.A.Solyak, "Gradient limitations in room temperature and superconducting acceleration structures," tech. rep., FERMILAB, 2007.

[7] J. Plouin, S. Chel, and G. Devanz, "Spl cavity design by cea-saclay," in *3rd SPL Collaboration Meeting*, 2009.

[8] J. et al., "Optimized rf design of 704 mhz beta=1 cavity for pulsed proton drivers," tech. rep., Saclay, 2011.

[9] C. Feneau, *Non-ferrous metals: from Ag to Zn.* Umicore, 2002.

[10] A. S. for Metals, *Materials properties handbook: Titanium alloys.* American Society for Metals, 2004.

[11] "Granta: C.e.s. selector material selection software," 2010.

[12] O.Capatina, G.Arnau, S.Atieh, G.Favre, F.Pillon, T.Renaglia, and W.Weingarten, "S.p.l. mechanical design and cavities construction," in *5th SPL Collaboration Meeting*, 2010.

[13] K. Zapfe-Dren, F. Herrmann, D. Hubert, and P. Schmser, "A new flange design for the superconducting cavities for tesla," in *Proc. of the 8th Workshop on RF Superconductivity*, 1997.

[14] C. Grimm, T. Arkan, M. Foley, T. Khabiboulline, and D. Watkins, "1.3 ghz rf nb cavity to ti helium vessel tig welding process at fermilab," in *Proceedings of SRF2009*, 2009.

[15] L. Lilje, *Experimental Investigations on Superconducting Niobium Cavities at Highest Radiofrequency Fields*. PhD thesis, Universitat Hamburg, 2001.

[16] L. Cartz, *Nondestructive Testing*. ASM International, 1995.

[17] A. S. for Metals, *Metals Handbook vol 17 - Nondestructive evalution and Quality Control*. American Society for Metals, 1996.

[18] P. E. Mix, *Introduction to Nondestructive Testing*. John Wiley and Sons, 2005.

[19] B. Raj, T. Jayakumar, and M. Thavasimuthu, *Practical Non - Destructive Testing*. Alpha Science International, 2002.

[20] J. Krautkrmer and H. Krautkrmer, *Ultrasonic testing of materials*. Springer - Verlag, 1990.

[21] J. J. Bozzola and L. D. Russell, *Electron Microscopy*. Jones and Barlett Publishers, 1999.

[22] "http://en.wikipedia.org."

[23] J. Goldstein, D. Newbury, D. Joy, C. Lyman, P. Echlin, E. Lifshin, L. Sawyer, and J. Michael, *Scanning Electron Microscopy and X-Ray Microanalysis*. Springer, third ed., 2003.

[24] H. Czichos, T. Saito, and L. Smith, *Springer Handbook of Materials Measurement Methods*. Springer, 2006.

[25] A. S. for Metals, *Metals Handbook vol 8 - Mechanical testing and evalution*. American Society for Metals, 2000.

[26] W. D. C. Jr, *Introduccion a la Ciencia e Ingenieria de los Materiales*, vol. 1. Reverte, 1995.

[27] J. Barralis and G. Maeder, *Prcis de mtallurgie*. AFNOR, 2005.

[28] B.E.Warren, *X-Ray Diffraction*. General Publishing Company, 1990.

[29] K. Mimura, Y. Ishikawa, M. Isshiki, and M. Kato, "Precise purity-evaluation of high-purity copper by residual resivity ratio," *Materials Transactions, JIM*, vol. 38, no. 8, p. 714 to 718, 1997.

[30] A. S. for Metals, *Metals Handbook Volume 2 Properties and selection Nonferrous Alloys and Pure Metals*. American Society for Metals, 1990.

[31] A. S. for Metals, *Metals Handbook vol 6 - welding and brazing*. American Society for Metals, 1987.

[32] H. Schultz, *Electron Beam Welding*. Abington publishing, 1993.

[33] Z.Charifoulline, "Residual resistivity ratio (rrr) measurements of lhc superconducting nbti cable strands," tech. rep., CERN, 2005.

[34] E.W.Collings, *Material Properties Handbook: Titanium Alloys*. ASM International, 2007.

[35] H.Padamsee, J.Knobloch, and T.Hay, *RF Superconductivity for Accelerators*. John Wiley and Sons, 1998.

[36] A.Zamiri, F.Pourboghrat, H.Jiang, T.R.Bieler, F.Barlat, J.Brem, C.Compton, and T.L.Grimm, "On mechanical properties of the superconducting niobium," *Materials Science and Engineering*, vol. A 435-436, pp. 658–665, 2006.

[37] Z. Sun and R. Karppi, "The application of electron beam welding for the joining of dissimilar metals: an overview," *Journal of Materials Processing Technology*, vol. 59, pp. 257 – 267, 1996.

[38] P.Villars and L.D.Calvert, *Pearson's Handbook of Crystallographic Data for Intermetallic Phases*. American Society for Metals, 1991.

List of Figures

List of Tables

A. Appendix

Niobium preparation for metallographic observation

VERSION: 1.0 DATE: 18.01.2011

The aim of this procedure is to give the detailed steps for a proper polishing of Niobium to achieve a mirror – like finish. It has been experienced with good results on a 3x20 mm sample.

	Cloth/ Abrasive paper	Abrasive/ Etching	Load (Lb)	Speed (rpm)/ Direction	Time
I.1	80, 180, 240, 320, 600, 1200 grit abrasive papers	/	3	150 / comp.	Until specimen surface is flat and show uniform scratches
I.2[1] **(Alternative)**	320 grit abrasive paper	/	6	150 / comp.	Until flat
II	ULTRAPAD	9 µm MetaDi Supreme	6	150 / contra.	10 min
III	VERDUTEX	3 µm MetaDi Supreme	6	150 / contra.	8 min
IV	CHEMOMET	Mixture of H_2O_2 (30%) + 0.05 µm MasterMet colloidal silica [1:5]	6	150 / contra.	5 min
ETCHING	/	solution # 160 of ASTM E407	/	/	30 – 45 s
EBSD	MICROCLOTH	Mixture of H_2O_2 (30%) + 0.05 µm MasterMet colloidal silica [1:5]	/	20% amplitude	1 hour

Table 1: Summary of the sample preparation

[1] First step of the specimen preparation for EBSD recommended by BUEHLER in a four – step procedure for refractory metals (other than Ti, Zr and Hf)

I) After putting the sample into resin, start grinding with the 80 grit abrasive paper until the sample is flat and the effects of the prior operations are removed. The next paper should remove the effects of the prior paper in a short time. The sequence followed was 80, 180, 240, 320, 600, 1200 grit abrasive papers (Fig. 1)

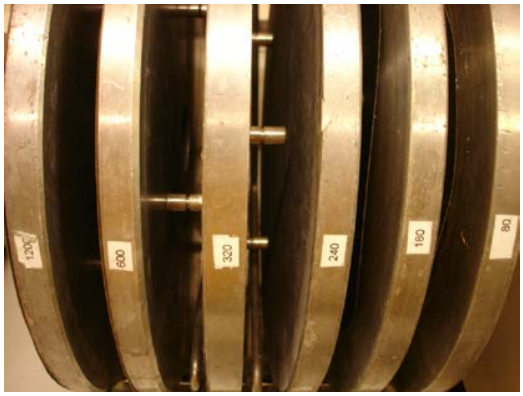

Figure 1: grit abrasive papers

If the grinding is done manually, the specimen has to be rotated 90 degrees between papers. If the grinding is done in an automatic device (Fig. 2), the following settings for each paper are recommended:

- Time: 1 min
- Speed (rpm) / direction: 150 / comp.
- Load (Lb): 3

The specimen surface should show uniform scratches before proceeding to the next step. If not, repeat current step with the same settings.


Figure 2: Automatic sample preparation device

Alternatively, good finishing can also be achieved with a simple automatic grinding using a 320 grit abrasive paper and the following settings

- Time: until flat
- Speed (rpm) / direction: 150 / comp.
- Load (Lb): 6

II) When the specimen surface is flat, use ULTRAPAD (Fig. 3) polishing cloth in the automatic polishing device with the following settings:

- Time: 10 min
- Speed (rpm) / direction: 150 / contra
- Load (Lb): 6

Add 8 drops of 9 µm MetaDi Supreme diamond suspension (Fig. 4) every 30 – 60 seconds.

Figure 3: ULTRAPAD polishing cloth

Figure 4: 9µm MetaDi Supreme diamond suspension

III) Use VERDUTEX (Fig. 5) polishing cloth in the automatic polishing device with the following settings:

- Time: 8 min
- Speed (rpm) / direction: 150 / contra
- Load (Lb): 6

Add 8 drops of 3 µm MetaDi Supreme diamond suspension (Fig. 6) every 30 – 60 seconds.

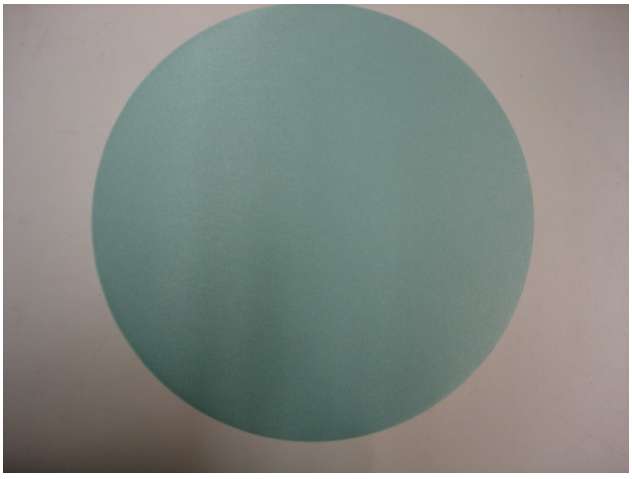

Figure 5: VERDUTEX polishing cloth

Figure 6: 3µm MetaDi Supreme diamond suspension

IV) Use CHEMOMET (Fig. 7) polishing cloth in the automatic polishing device with the following settings:

- Time: 5 min
- Speed (rpm) / direction: 150 / contra
- Load (Lb): 6

Add 1 spray (approximately 5 ml) of a mixture of 1 part H_2O_2 (30%) to 5 parts 0.05 µm MasterMet colloidal Silica (Fig. 8) every 30 – 60 seconds.

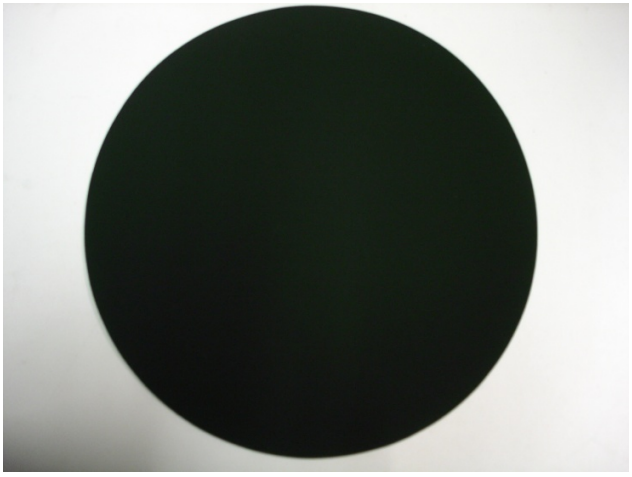

Figure 7: CHEMOMET polishing cloth

Figure 8: 0.05µm MasterMet colloidal Silica suspension

V.1) For grain size determination, immerse the sample for 30 – 45 seconds in solution # 160 of ASTM E407 (Fig. 9).

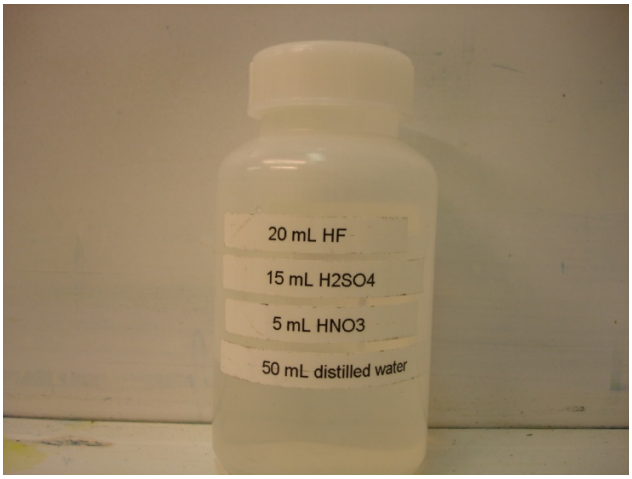

Figure 9: etchant #160 of ASTM E407

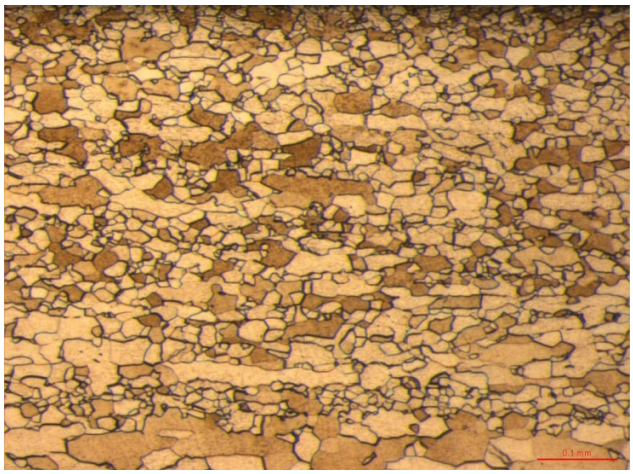

Figure 10: Niobium after 30s of etching

V.2) For EBSD observation, one hour of vibratory polishing at 20% amplitude using the sample holder with no extra weight, a MICROCLOTH pad and the same mixture used in IV) improves the band contrast of the Kikuchi patterns.

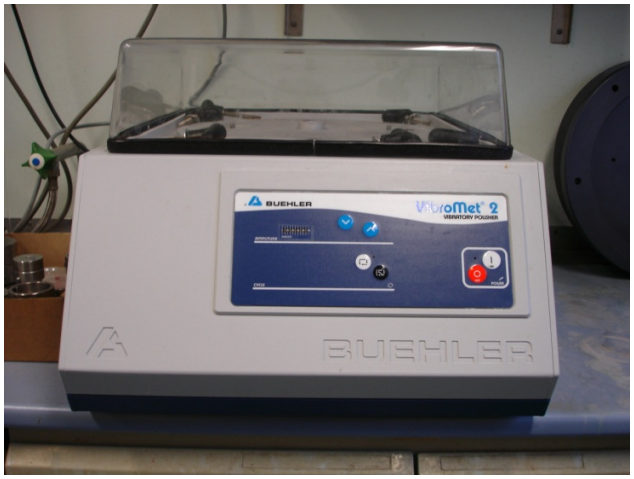

Figure 11: VibroMet vibratory polishing device

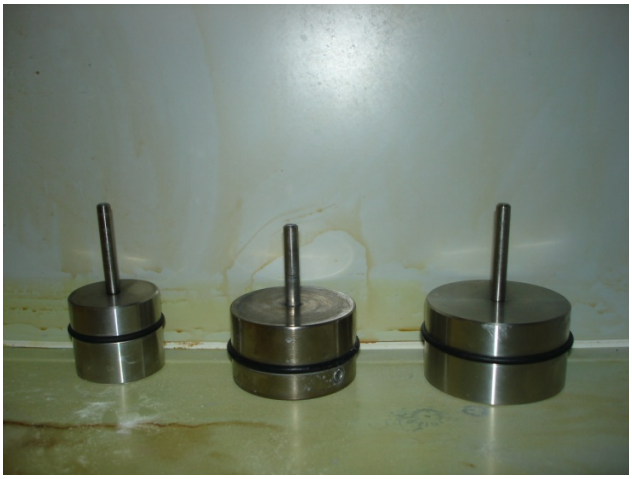

Figure 12: Sample holders for VibroMet

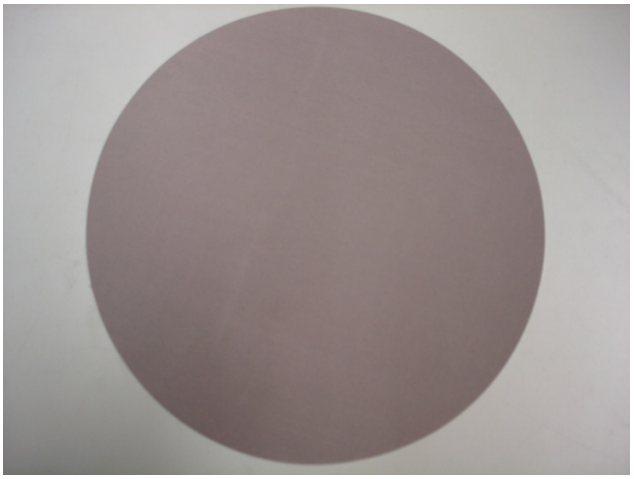

Figure 13: MICROCLOTH polishing cloth